NEUROSCIENCE

Beyond volume: Unraveling the genetics of human brain geometry

Sabrina A. Primus[1,2,3], Felix Hoffstaedter[4,5], Federico Raimondo[4,5], Simon B. Eickhoff[4,5], Juliane Winkelmann[1,3,6,7], Konrad Oexle[1,2,3]*†, Kaustubh R. Patil[4,5]*†

Brain geometry affects brain function. A quantitative encoding of form is provided by the Laplace-Beltrami operator's spectrum of eigenvalues (LBS). We examined LBS genetics of 22 subcortical brain structures and cerebellum in 19,862 healthy White-British UK Biobank participants by multivariate genome-wide association study on the first 49 eigenvalues each. Controlling for surface and volume, we identified 80 unique variants influencing the shapes of one or several structures, with the highest yield (37 variants) for brain stem. The previously known influence of several of these loci on basic morphology, such as volume, is thus shown to also influence complex shape. Known associations of observed loci with blood pressure, neurodegeneration, alcohol consumption, and mental disorders hint at preclinical stages of these conditions potentially mediating the genetic effect on brain morphology. Significant correlations between LBS of several brain structures and the polygenic risks of hypertension, ischemic stroke, and schizophrenia evince brain shapes as early biomarkers.

INTRODUCTION

The human brain comprises an intricate constellation of diverse substructures, each of which has specific functions and forms complex interactions with other parts of the brain. Investigating the morphological properties of these substructures and deciphering their genetic underpinnings is imperative for advancing our understanding of the human brain in health and disease. Previous genetic studies have investigated crude parameters such as volume and surface area (*1*–*5*). The genetics of the intricate shapes of brain structures, however, remain largely unexamined, representing a gap in comprehensive understanding of brain anatomy.

The structures within the human brain exhibit a range of shapes, from the more spherical amygdala to the elongated hippocampus. Basic metrics such as volume and surface area do not adequately capture the nuanced details of these shapes and thus fall short of providing a sufficient description of their morphology. There is evidence for a high interindividual variance in these intricate details, with a substantial proportion being heritable (*6*–*8*). Initial efforts to delve into the genetic underpinning of this heritable aspect used techniques like voxel-based analysis in combination with dimension reduction methods (*9*, *10*) or global-to-local representations of brain shapes (*11*, *12*). Each of these techniques carries its own challenges, including reduced robustness and accuracy because of suboptimal image registration, high computational effort, or a lack of physical interpretability as a result of dimensionality reduction or a prohibitive dimensionality of image-derived features.

The Laplace-Beltrami operator provides a multivariate spectral representation of a shape, capturing its characteristics in detail (*13*, *14*). The Laplace-Beltrami spectrum (LBS), a set of ordered eigenvalues, is obtained by solving the Helmholtz equation, a time-independent form of the wave equation, on a Riemannian manifold that can be the surface of a given brain structure. Solutions are decomposed into eigenfunctions (also referred to as "eigenmodes") and their corresponding eigenvalues, representing the natural vibrations and their squared frequencies, respectively, on the manifold underlying the shape, akin to the harmonic frequencies of the membrane of a drum (fig. S1) (*15*). Each sound or other vibration of a membrane can be represented as a weighted sum of its eigenmodes, relating closely to the theory of spectral analysis in Fourier series. Necessarily, the eigenmodes are strongly linked to a shape's geometry, as visualized in a seminal experiment by Chladni (*16*) using vibrating plates. It has been asked since then whether a shape can be represented by a unique series of eigenvalues or, metaphorically, whether the shape of a drum can be heard (*17*). While the answer is affirmative for one-dimensional shapes whose lengths are made audible by the harmonics or pure tones of string instruments, for instance, this is not true in general for shapes with more than one dimension as there exist isospectral shapes (*18*). Nevertheless, the known counterexamples appear to be rare (*13*), and under certain symmetry assumptions, a unique assignment is possible (*19*). Consequentially, a relatively small subsequence (e.g., 50 eigenvalues) of the increasingly ordered spectrum contains enough geometric information to describe a shape uniquely enough by adequately capturing its curvatures (*13*, *15*, *20*, *21*), although the spectrum usually contains an infinite number of eigenvalues. Following Ge *et al.* (*6*), we refer to this subsequence as the LBS [also known as Shape-DNA (*13*)]. This multidimensional intrinsic shape representation, as an isometric invariant, is independent of rotation, translation, and scaling of the coordinate system, eliminating the need for error-prone interindividual image registration, and behaves continuously with any change in the manifold (*13*). Recently, there has been considerable interest in using geometric eigenmodes to explain shape-associated biological mechanisms (*22*). The LBS, however, appears to be a more straightforward shape descriptor that is computed efficiently (*21*) and thus well suited for

[1]Institute of Neurogenomics, Helmholtz Zentrum München, German Research Center for Environmental Health, Neuherberg, Germany. [2]Neurogenetic Systems Analysis Group, Institute of Neurogenomics, Helmholtz Zentrum München, German Research Center for Environmental Health, Neuherberg, Germany. [3]Institute of Human Genetics, TUM School of Medicine and Health, Technical University of Munich, Munich, Germany. [4]Institute of Neuroscience and Medicine, Brain & Behaviour (INM-7), Research Centre Jülich, Jülich, Germany. [5]Institute of Systems Neuroscience, Medical Faculty, Heinrich Heine University Düsseldorf, Düsseldorf, Germany. [6]Munich Cluster for Systems Neurology (SyNergy), Munich, Germany. [7]German Center for Mental Health (DZPG), partner site Munich-Augsburg, Munich-Augsburg, Germany.
*Corresponding author. Email: konrad.oexle@helmholtz-munich.de (K.O.); k.patil@fz-juelich.de (K.R.P.)
†These authors contributed equally to this work.

large-scale genome-wide association studies (GWASs), which require a quantitative representation of the shape of brain structures at the individual level.

By performing GWAS, we aimed to reveal information on gene loci that contribute to the heritability of brain morphology as quantified by LBS. We derived the LBSs of 22 different brain structures from a large magnetic resonance imaging (MRI) dataset provided by the UK Biobank (UKB). To reveal shape-specific signals, we controlled for global characteristics such as brain volume and surface area. Because all eigenvalues in an LBS contribute to the description of the respective shape, it is important to study them jointly while accounting for their mutual dependencies. To achieve this, we used the state-of-the-art multivariate GWAS tool MOSTest (*2*), which accounts for the pairwise correlations between eigenvalues and has increased power for detecting genetic associations by considering their joint distribution. Our study focused on subcortical structures, brain stem, and cerebellum, in keeping with several studies that studied the genetics of their volumes (*2*, *5*, *23*–*25*). These parts of the brain are involved not only in learning and decision-making processes (*26*) but also in hotspots of various brain disorders (*7*, *23*–*25*, *27*). We identified specific genetic influences on their shapes, investigated genetic asymmetries and similarities among structures, obtained precise estimates of the heritability of these shapes, and performed genetic correlation and enrichment analyses with respect to biological pathways, traits, and diseases.

RESULTS

Multivariate genome-wide analyses

MOSTest on the LBS of each of the 22 brain structures in 19,862 healthy, unrelated, White-British individuals (10,427 female, with mean age ± SD of 64.3 ± 7.4 years) yielded a total of 148 significant single-nucleotide polymorphisms (SNPs; Bonferroni-corrected for multiple testing $P < 1/22 * 5 \times 10^{-8} = 2.27 \times 10^{-9}$), which were each independent [linkage disequilibrium (LD) of $r^2 < 0.6$] in their respective LBS GWAS. Some of them were significant in multiple brain structures. Thus, across all 22 GWASs, there were 80 unique SNPs independently associated with the shape of at least one brain structure (table S1 and figs. S2 to S4).

Using FUMA (*28*) for clumping the results of each brain structure (see Materials and Methods), we identified 62 genomic risk loci in total, of which 48 were shared by at least 2 of the 22 brain structures (Fig. 1). The largest number of independent significant SNPs was found for the brain stem (37) (Fig. 2B), followed by left cerebellum white matter (29). Only the amygdala did not show any significant signals after Bonferroni correction. The strongest signal was observed for lead SNP rs13107325 on chromosome 4 with a *P* value of 2.15×10^{-74} in association with the LBS of the left cerebellum white matter. This SNP association was observed most frequently, appearing in 14 of the 22 brain structures.

Forty-nine of the 80 independent SNPs, either themselves or via a proxy variant $(r^2 \geq 0.6)$, have previously been identified in GWASs on brain shape–related traits (e.g., volume, surface area, or cortical thickness; table S2) and are listed in the GWAS catalog implemented in FUMA. Of these 80, 13 have been associated exclusively with other traits (not brain shape–related), and 18 were not related to any GWAS catalog entry (table S1).

Functional annotations of genomic risk loci

We annotated our results using ANNOVAR (*29*) as implemented in FUMA. Of the 80 independent significant SNPs, 3 were exonic, 27 were intronic, and 33 were in intergenic regions (Fig. 2A and

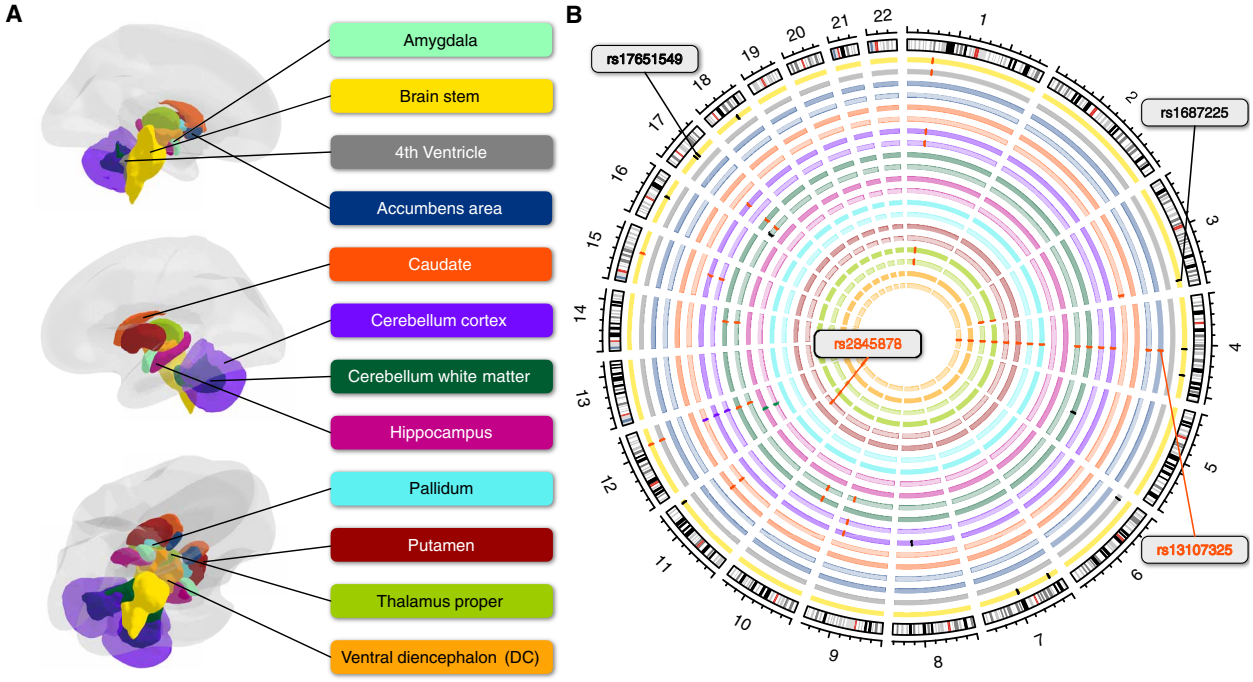

Fig. 1. Overview of genomic risk loci in different brain structures. (**A**) Anatomical representation of the subcortical brain structures assessed in the present study. (**B**) Circular plot indicating the genomic risk loci derived by MOSTest GWAS on each brain structure (with the exception of the amygdala, which did not provide a genome-wide significant signal). Bilateral structures are represented on neighboring circles, having the same colors as in (A), with the right-side structure represented more centrally and lighter. If multiple structures share a locus, the bars indicating their positions on the respective circles have the same color.

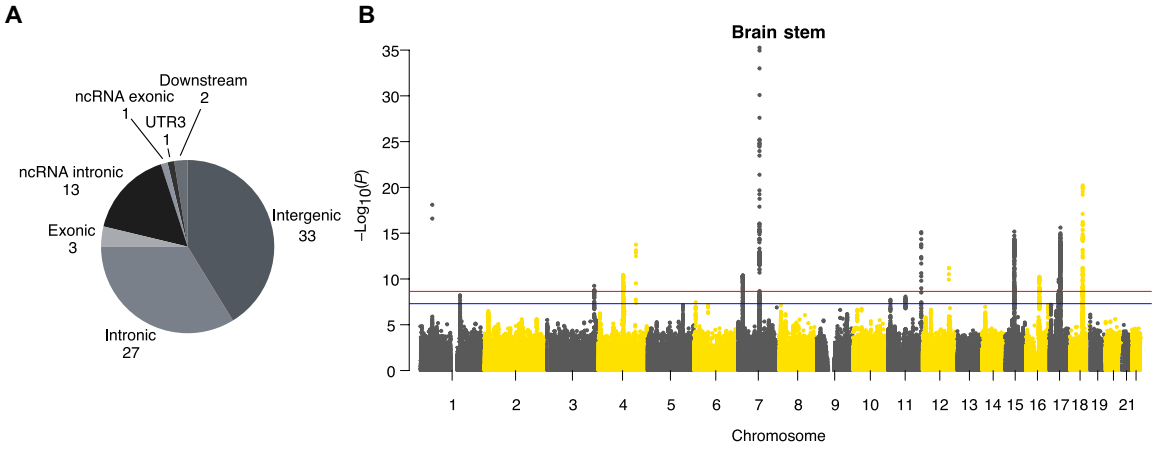

Fig. 2. SNP-based associations with the LBS. (**A**) Pie chart showing the frequency of functional annotations of all 80 independent significant SNPs. (**B**) Manhattan plot of multivariate MOSTest results of the brain stem with corrected and noncorrected genome-wide significant thresholds [$P = 2.27 \times 10^{-9}$ (red line) and $P = 5 \times 10^{-8}$ (blue line)].

table S3). All three exonic variants (rs13107325, rs1687225, and rs601558) were nonsynonymous, each having a combined annotation-dependent depletion (CADD) score higher than 15.23 and belong, therefore, to the 3% most deleterious SNPs (*30*). We further found 28 exonic nonsynonymous (ExNS) variants in LD $\left(r^2 \geq 0.6\right)$ with one of the independent significant SNPs, with 17 of them having a CADD score higher than 15.23 or a Regulome DB score (RDB; small scores indicating a high likelihood of being a regulatory SNP) lower than 2 (Table 1 and table S4).

The pleiotropic missense variant rs13107325, as mentioned above, affects the metal transporter *SLC39A8* and is, with a CADD score higher than 20 (23.1), among the 1% most deleterious SNPs. While ClinVar (*31*) and AlphaMissense (*32*) classify this pleiotropic variant as benign, it is a well-known risk factor for schizophrenia (SCZ) (*33*–*35*) and has also been found in conjunction with inflammation-based diseases like Crohn's disease (*36*) and blood pressure (*37*), as well as brain imaging phenotypes (*9*).

VWA5B2 on chromosome 3 comprises the ExNS missense variant rs1687225, an independent significant SNP associated with brain stem LBS ($P = 5.6 \times 10^{-10}$). The CADD score of this variant is relatively high (*19*), but this SNP is not reported in ClinVar and AlphaMissense predicts it to be likely benign. Of note, the variant is a brain expression quantitative trait locus (eQTL) for different genes and an independent brain cis-eQTL for *VWA5B2* itself according to GTEx (version 8) (table S5).

The ExNS missense variant rs601558 on chromosome 8 was significantly associated with the LBS of the left cerebellum cortex ($P = 8.0 \times 10^{-11}$) and is contained in *RSPO2*, for which it is also a brain eQTL. Despite a high CADD score of 22, this variant is classified as benign by ClinVar and AlphaMissense.

Despite its benign classification by ClinVar and AlphaMissense, rs17651549 in *MAPT* on chromosome 17, which was associated with the brain stem LBS at $P = 1.0 \times 10^{-13}$, had the highest CADD score (26.8) among the ExNS variants. It was in nearly complete LD ($r^2 = 0.96$) with the lead SNP rs568589031 (brain stem, $P = 2.4 \times 10^{-16}$) of this large genomic risk locus that included altogether six ExNS SNPs, which, according to the CADD score, all belong to the 3% most deleterious SNPs (Table 1) and act as brain eQTLs of *CRHR1*, *SPPL2C*, *MAPT*, and *KANSL1*. Because of its high linkage, this large genomic region, also referred to as *MAPT* locus, is known to be highly complex (*38*) and we observed 18 ExNS SNPs being brain eQTLs of 17 protein-coding genes in total (table S6).

Asymmetry and similarity of brain structures

To assess possible genetic asymmetries and similarities of brain structures, we compared the *P* values of the 80 unique independent SNPs between structures and hemispheres (table S7). Applying a conservative Bonferroni correction for 80 * 22 comparisons to the nominal threshold of 0.05, we found five genome-wide significant ($P < 2.27 \times 10^{-9}$) SNPs for cerebellum white matter and one for putamen that were not significant in the respective contralateral structures. At nominal significance, only the intron variant rs2845878 in *FAT3*, which came up in the GWAS on right putamen, lacked symmetry. Proxy variants of rs2845878 $\left(r^2 \geq 0.6\right)$ have been linked to the mean volume of caudate and putamen according to the GWAS catalog (*4*). Principal components analysis (PCA) of $-\log_{10}$-transformed *P* values of these 80 SNPs showed a high level of symmetry and similarity in genetic signals (Fig. 3 and table S8): All subcortical structures as well as the cerebellum cortex were mapped close to each other in this principal component (PC) space, independent of their hemispherical assignment. Moreover, most structures shared genetic architecture according to their placement adjacent to each other as in case of the basal ganglia, for instance. However, the brain stem, cerebellum white matter, and hippocampus were substantially distanced from the others in at least one of the first three PCs. The hippocampus was probably notable for its dissimilar pattern of few associated SNPs, while the particular position of the brain stem and cerebellum white matter could be due to their highly significant signals in addition to their quantity.

When investigating genetics that were similar for several structures, the ExNS variant rs13107325 in *SLC39A8*, along with several others within the same risk locus on chromosome 4, the intergenic SNP rs6658111 on chromosome 1, and the intronic variant rs12146713 in *NUAK1* on chromosome 12 emerged as the most frequently shared independent SNPs. After Bonferroni correction for 80 * 22 comparisons, these three were significant in 10 to 15 structures and

Table 1. Exonic nonsynonymous variants in LD ($r^2 \geq 0.6$) with one of the independent significant SNPs across all brain structures. Variants are listed with noneffect allele (NEA), effect allele (EA), effect allele frequency (EAF), minimal *P* value (minP) across all structures, CADD and RDB scores, most likely affected gene, and the independent significant SNPs (IndSigSNP) to which they are linked most strongly as indicated by the correlation value r^2. The respective IndSigSNP may differ between brain structures according to the structure-specific GWAS results. Bold typing of a variant indicates genome-wide significance in at least one brain structure. Variants in italics are independent significant SNPs.

rsID	Position	EA	NEA	EAF	MinP	CADD	RDB	Gene	Brain structure (IndSigSNP, r^2)
rs1687225	chr3:183948663	A	G	0.23	6×10^{-10}	19.0	4	*VWA5B2*	Brain stem (***rs1687225***, 1.00)
rs902417	chr3:183951431	T	C	0.25	7×10^{-08}	15.4	5	*VWA5B2*	Brain stem (***rs1687225***, 0.86)
rs3733197	chr4:102839287	A	G	0.35	2×10^{-06}	14.2	7	*BANK1*	Left cerebellum white matter (***rs114614648***, 0.72)
rs13107325	chr4:103188709	T	C	0.08	2×10^{-74}	23.1	5	*SLC39A8*	Accumbens area (right + left: ***rs13107325***, 1.00); cerebellum cortex (right + left: ***rs13107325***, 1.00); cerebellum white matter (right + left: ***rs13107325***, 1.00); pallidum (right + left: ***rs13107325***, 1.00); putamen (right + left: ***rs13107325***, 1.00); ventral DC (right + left: ***rs13107325***, 1.00); thalamus proper (right: ***rs13107325***, 1.00; left: ***rs13135092***, 0.93)
rs7800072	chr7:84628989	G	T	0.32	3×10^{-08}	18.3	5	*SEMA3D*	Brain stem (***rs10247311***, 0.90)
rs601558	chr8:108970367	G	A	0.34	8×10^{-11}	22.0	5	*RSPO2*	Left cerebellum cortex (***rs601558***, 1.00)
rs36045050	chr14:69257858	T	C	0.26	8×10^{-09}	7.0	2b	*ZFP36L1*	Cerebellum white matter (right: ***rs1547050***, 0.74; left: ***rs12435718***, 0.73)
rs4646626	chr15:58256127	T	C	0.46	6×10^{-15}	19.7	NA	*ALDH1A2*	Brain stem (***rs1061278***, 0.91); cerebellum cortex (right: ***rs3742960***, 0.92; left: ***rs3742959***, 0.92)
rs1877031	chr17:37814080	A	G	0.33	1×10^{-06}	23.1	NA	*STARD3*	Brain stem (***rs2271308***, 0.80)
rs1058808	chr17:37884037	G	C	0.33	1×10^{-07}	23.5	5	*ERBB2*	Brain stem (***rs2271308***, 0.64)
rs12949256	chr17:43507297	T	C	0.19	1×10^{-08}	15.0	4	*ARHGAP27*	Brain stem (***rs568589031***, 0.70)
rs16940674	chr17:43910507	T	C	0.24	1×10^{-13}	17.6	1f	*CRHR1*	Brain stem (***rs568589031***, 0.96)
rs16940681	chr17:43912159	C	G	0.24	1×10^{-13}	5.0	4	*CRHR1*	Brain stem (***rs568589031***, 0.96)
rs62621252	chr17:43922942	C	T	0.24	6×10^{-14}	6.3	5	*SPPL2C*	Brain stem (***rs568589031***, 0.96)
rs62054815	chr17:43923266	A	G	0.24	1×10^{-13}	0.0	5	*SPPL2C*	Brain stem (***rs568589031***, 0.96)
rs12185233	chr17:43923654	C	G	0.24	5×10^{-14}	23.5	1f	*SPPL2C*	Brain stem (***rs568589031***, 0.95)
rs12185268	chr17:43923683	G	A	0.24	1×10^{-13}	8.7	1f	*SPPL2C*	Brain stem (***rs568589031***, 0.96)
rs12373123	chr17:43924073	C	T	0.24	1×10^{-13}	23.3	1f	*SPPL2C*	Brain stem (***rs568589031***, 0.96)

(*Continued*)

Table 1. (*Continued*)

rsID	Position	EA	NEA	EAF	MinP	CADD	RDB	Gene	Brain structure (IndSigSNP, r^2)
rs12373139	chr17:43924130	A	G	0.24	1×10^{-13}	4.0	1f	*SPPL2C*	Brain stem (***rs568589031***, 0.96)
rs12373142	chr17:43924200	G	C	0.24	7×10^{-13}	7.5	1f	*SPPL2C*	Brain stem (***rs568589031***, 0.96)
rs63750417	chr17:44060775	T	C	0.24	1×10^{-13}	11.9	5	*MAPT*	Brain stem (***rs568589031***, 0.96)
rs62063786	chr17:44061023	A	G	0.24	9×10^{-14}	7.9	5	*MAPT*	Brain stem (***rs568589031***, 0.96)
rs62063787	chr17:44061036	C	T	0.24	1×10^{-13}	0.2	5	*MAPT*	Brain stem (***rs568589031***, 0.96)
rs17651549	chr17:44061278	T	C	0.24	1×10^{-13}	26.8	1f	*MAPT*	Brain stem (***rs568589031***, 0.96)
rs10445337	chr17:44067400	C	T	0.24	2×10^{-13}	19.2	1f	*MAPT*	Brain stem (***rs568589031***, 0.96)
rs62063857	chr17:44076665	G	A	0.24	1×10^{-13}	1.5	7	*STH*	Brain stem (***rs568589031***, 0.96)
rs34579536	chr17:44108906	G	A	0.24	2×10^{-13}	14.4	3a	*KANSL1*	Brain stem (***rs568589031***, 0.96)
rs34043286	chr17:44117119	G	A	0.24	1×10^{-13}	21.0	4	*KANSL1*	Brain stem (***rs568589031***, 0.96)

nominally significant in 19 and 20 structures (table S7). Apart from the pleiotropic rs13107325, the other two variants have so far only been linked to various brain shape–related traits such as volume, surface area, and cortical thickness according to the GWAS catalog as implemented in LDtrait (table S9) (*39*). rs12146713 and rs13107325 have also recently been linked to structural connectivity measures (*40*), which supports the notion that they have an overarching effect on brain structuring.

Gene mapping and gene enrichment analysis

We first annotated all SNPs passing quality control (QC) to 18383 protein-coding genes using MAGMA (*41*) and calculated a *P* value for each gene by applying the SNP-wise mean model (see Materials and Methods). The brain stem stood out with 20 protein-coding genes being significantly associated with its shape in the gene-based analysis after Bonferroni correction for 22 brain structures and 18,383 protein-coding genes [$P < 0.05/(22 * 18{,}383)$] (Fig. 4A). Here, *CRHR1* showed the strongest signal ($P = 5.2 \times 10^{-15}$). This gene belongs to the extended *MAPT* locus mentioned above, which came up as generally highly significant and has, together with *MAPT*, which encodes for the microtubule-associated protein tau, often been associated with neurodegenerative disorders (*42*, *43*).

Next, we used PoPS (*44*) for gene prioritization, a tool that assigns polygenic priority scores to each gene by fitting their MAGMA *z*-scores based on trait-relevant gene features extracted from cell type–specific gene expressions, biological pathways, and protein-protein interactions. Because PoPS works best when combined with orthogonal methods, we also mapped each SNP to the nearest genes. Reranking the genes according to the mean of the two ranks that resulted from the two methods, we prioritized all genes with rank ≤ 2 at each locus (see the Materials and Methods and table S10).

On the basis of these genes, a gene set enrichment analysis was conducted using FUMA's Gene2Func method. For bilateral brain structures, the two gene sets were joined in this analysis because of similar genetic architectures on both sides (see above and Fig. 3). Afterward, the overlap and degree of overrepresentation of all prioritized genes in predefined gene sets were examined (Figs. 4 to 6 and fig. S5).

For the brain stem, Gene2Func identified gene sets linked to multiple biological processes listed in the Gene Ontology (GO) Resource, which are involved in cell and nervous system development and regulation (Fig. 4B). Gene sets were also linked to brain morphology and lung function according to the GWAS catalog (Fig. 5A). Moreover, brain stem shape–related genes were enriched among genes differentially expressed in early infancy brain tissue (fig. S6).

At the locus of the most significant SNP in this study, rs13107325, two genes were usually prioritized, *BANK1* and *SLC39A8* (table S10). The previously known pleiotropy of this genomic region was confirmed by the diversity of our enrichment results, which included adventurousness, hypertension (HT), multisite chronic pain, general cognitive ability, and alcohol consumption (Fig. 6). In particular, the overlap with alcohol consumption was prominent.

Together with 23 other genes, these two genes were also prioritized in the case of cerebellum white matter. However, as a result of the larger number and variety of genes, the overlap of *BANK1* and *SLC39A8* with GWAS catalog gene sets remained above the significance threshold. Instead, the other genes, primarily prioritized in the case of cerebellar white matter, caused enrichments for several regulatory pathways of GO biological processes associated with neurological and developmental processes (Fig. 5B). Genes prioritized for hippocampus shape revealed a complete overlap with genes associated with its fissure but only a partial overlap with its total volume

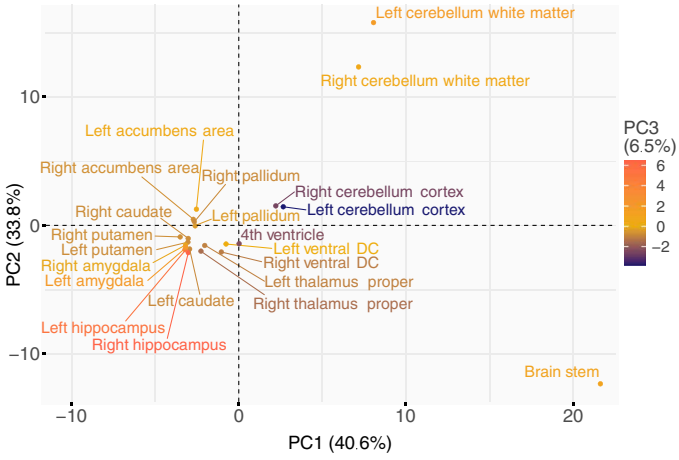

Fig. 3. PCA of $-\log_{10}$-scaled *P* values of the 80 independent significant SNPs across all structures. The first two PCs are plotted along the axes, while the third PC is color coded. Percentages in parentheses indicate the corresponding explained variances.

(<20%), reinforcing the validity and utility of our shape analysis (Fig. 5C).

Associations with polygenic risk scores

To investigate associations between brain-related traits and the LBS of individual brain structures, we extracted polygenic risk scores (PRSs) from UKB for Alzheimer's disease (AD), bipolar disorder (BD), ischemic stroke (ISS), multiple sclerosis (MS), Parkinson's disease (PD), and SCZ. Because of results of our gene set enrichment analyses (see above), we also included the PRS for alcohol use disorder (ALC) as available in the PGScatalog. Ten of the pairwise partial correlations (adjusted for covariates; see Materials and Methods) between the PRSs were significant (Bonferroni-corrected $P < 0.05$), most prominently between SCZ and BD (Pearson's $r = 0.37$, $P < 1 \times 10^{-300}$), ALC and SCZ ($r = 0.12$, $P = 1.5 \times 10^{-60}$), and ALC and BD ($r = 0.09$, $P = 1.7 \times 10^{-38}$) (tables S11 to S13).

Following Sha *et al.* (*45*), we performed canonical correlation analysis (CCA) between the LBS of each of the 22 brain structures and each of those PRSs (see Materials and Methods and table S14). Here, the CCA determined a linear combination of the eigenvalues of an LBS (i.e., the canonical variable), which correlates maximally with the PRS across all examined individuals. We found 31 significant correlations after Benjamini-Hochberg (*46*) correction ($P < 0.05$) within each PRS, 11 of which also stayed significant after additional Bonferroni correction for six independent PRSs (two-level correction) and 6 of which survived an overall Bonferroni correction for 22 * 6 tests (Fig. 7). As a balance between false discoveries and sensitivity, we chose this two-level correction to further investigate associations between PRSs and brain structures. Significant correlations ranged from 0.065 to 0.080 (mean, 0.070). While we found several highly significant correlations with various brain structures for ISS and SCZ, the polygenetic risk for BD and PD did not correlate with any brain shape at all. This is particularly notable because the PRS of BD and SCZ had substantial correlation (see above). The PRSs of AD, ALC, and MS indicated only suggestive correlations with LBSs. Empirical significance testing using 100,000 permutations of sample IDs for each pair of PRS and brain structure resulted in the same pattern of significant correlations (fig. S7).

To interpret these findings at the level of the eigenvalues, we calculated the mean loadings in each CCA and counted the number of negative and positive values (table S15). We noticed that in some results, it was possible to assess a common direction of effects. Among all significant results, the right ventral diencephalon (DC) revealed the strongest (i.e., largest absolute) mean loading of −0.295 with 96% of all eigenvalues having a negative correlation with the canonical variable and, in the case of a common direction, with the PRS of SCZ. This finding suggested that a person may have a higher genetic risk for SCZ if the right ventral DC is shaped in such a way that its eigenvalues (frequencies) are lower. This, for example, can be the case for a smoother surface or a less curved shape. A similar deduction in the case of brain stem suggested that a less smooth or more curved shape shows a higher risk for ISS (mean loading of 0.186 with ~92% loadings positive). Although most correlations remained above the significance threshold, clustering of the mean loadings showed similar tendencies for both hemispheres, suggesting no asymmetric behavior (fig. S8).

Heritability

We used SCORE (*47*) to estimate the univariate heritability of each eigenvalue, which uses the individual genotype data similar to the analysis by Ge *et al.* (*6*). We also calculated the multidimensional heritability (see Materials and Methods) (*6*) for each brain structure (Table 2 and table S16). Overall, the multidimensional heritability of the LBS was significant for all examined brain structures {Bonferroni corrected for 22 structures; range h^2: [9.5%, 29.6%]; mean ± SD = 17.2 ± 5.6%}. The highest heritability was found for the caudate (left: 29.6%; right: 27.3%) as well as for the brain stem (28.2%). We further computed the multidimensional LBS heritability for combined structures to compare them with the results from Ge *et al.* (Table 2 and fig. S9) and found a positive linear correlation (Pearson's $r = 0.735$, $P = 0.038$). However, Spearman's ρ did not reach statistical significance ($\rho = 0.714$, $P = 0.058$), suggesting a nonmonotonic relationship. Excluding the fourth ventricle, which may be an outlier in the study of Ge *et al.* because of its large standard error and very low heritability, both results affirm a significant correlation ($r = 0.844$, $P = 0.017$, and $\rho = 0.786$, $P = 0.048$). We further conducted a Wald test for different heritability in each combined brain structure with $H_0: h^2 = h^2_{Ge}$, which could not be rejected at a 0.05 significance threshold for any of the structures (see Materials and Methods and table S17), implying that our heritability estimates do not differ significantly from those of Ge *et al.*

Replication

On the 20% replication sample ($N = 4961$), we performed a replication analysis of the 80 independent SNPs (see Materials and Methods). For each brain structure, we only investigated those variants of the 80 SNPs that had also shown Bonferroni-corrected genome-wide significance in the respective discovery GWAS. We replicated 51.4% (76 of 148) of all significant associations of these 80 SNPs at a 0.05 significance level after false discovery rate (FDR) correction and 60.8% (90 of 148) at the nominal significance level (table S18). Hence, using a similar replication sample size, van der Meer *et al.* (*2*), who introduced MOSTest in their study on brain volumes, replicated 33% fewer signals than we did.

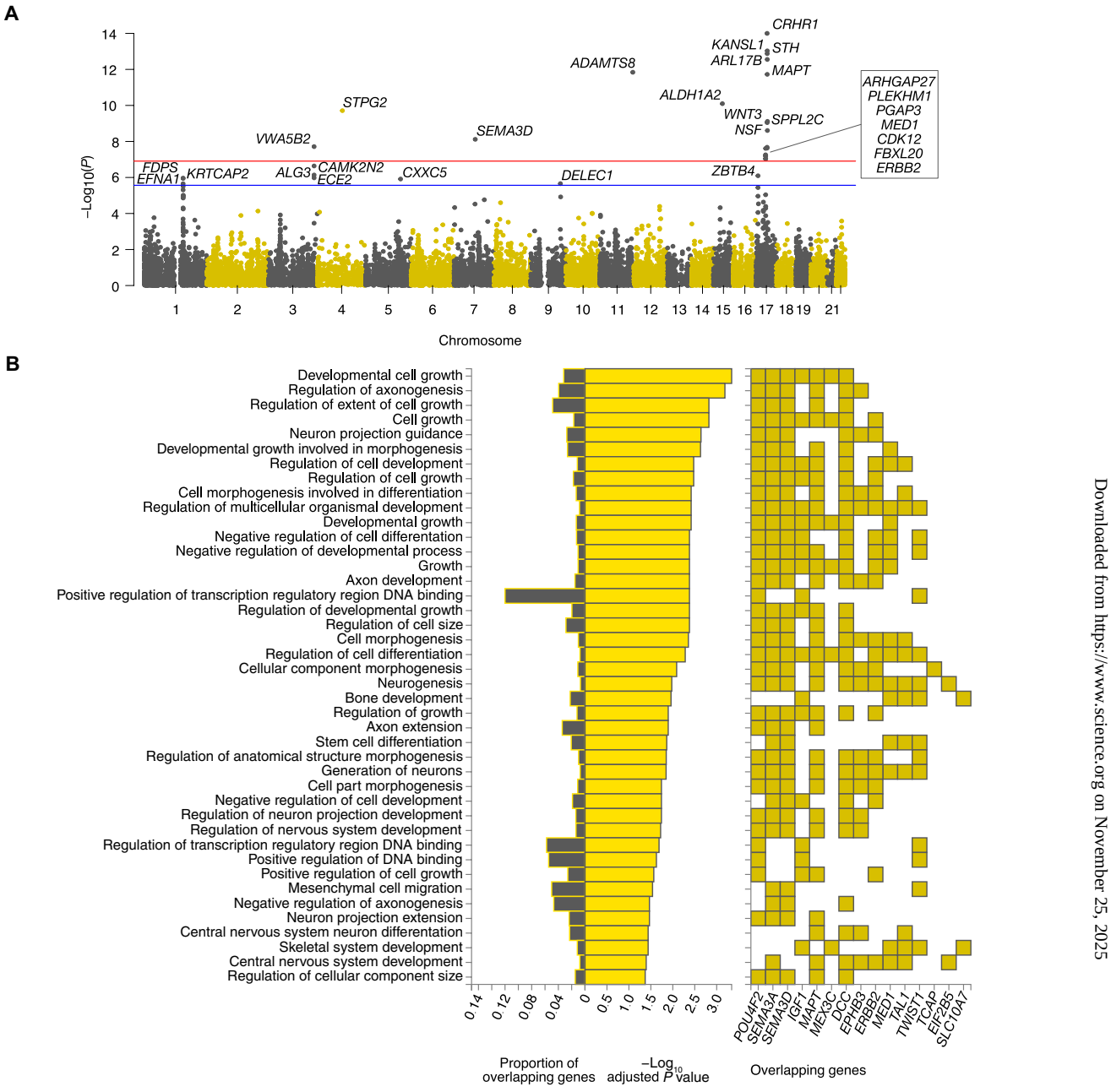

Fig. 4. Gene analysis and enrichment in the brain stem. (**A**) Manhattan plot of MAGMA gene analysis of brain stem results using the SNP-wise mean model with corrected and noncorrected gene-wide significant thresholds [$P = 0.05/(22 * 18{,}383)$ (red line) and $P = 0.05/18{,}383$ (blue line)]. (**B**) Hypergeometric tests of overrepresentation and overlap of prioritized genes with predefined gene sets (GO biological processes from MsigDB c5) using FUMA Gene2Func. *P* values were corrected by the Benjamini-Hochberg method for multiple testing.

We further checked all 148 significant associations of independent SNPs with brain structures and their replication *P* values with respect to their novelty in brain shape–related GWASs. Thirty-one of 80 independent SNPs across all brain structures have not been previously associated with any brain shape–related trait (see the "Multivariate genome-wide analyses" section). Among the 148 independent significant SNP brain structure associations, these 31 SNPs were involved in 36 associations. A total of 30.5% (11 of 36) of these associations replicated after FDR correction at a significance threshold of 0.05, whereas 50.0% (18 of 36) replicated at the nominal significance threshold ($P < 0.05$). Among the other 112 associations, already associated with brain shape–related traits, we replicated 58.0% (65 of 112) and 64.3% (72 of 112), respectively. Fisher's test showed a nonsignificant difference ($P = 0.169$) of nominal replication rates between novel and already reported genetic associations and a significant difference ($P = 0.007$) of the FDR-corrected replication rates. We

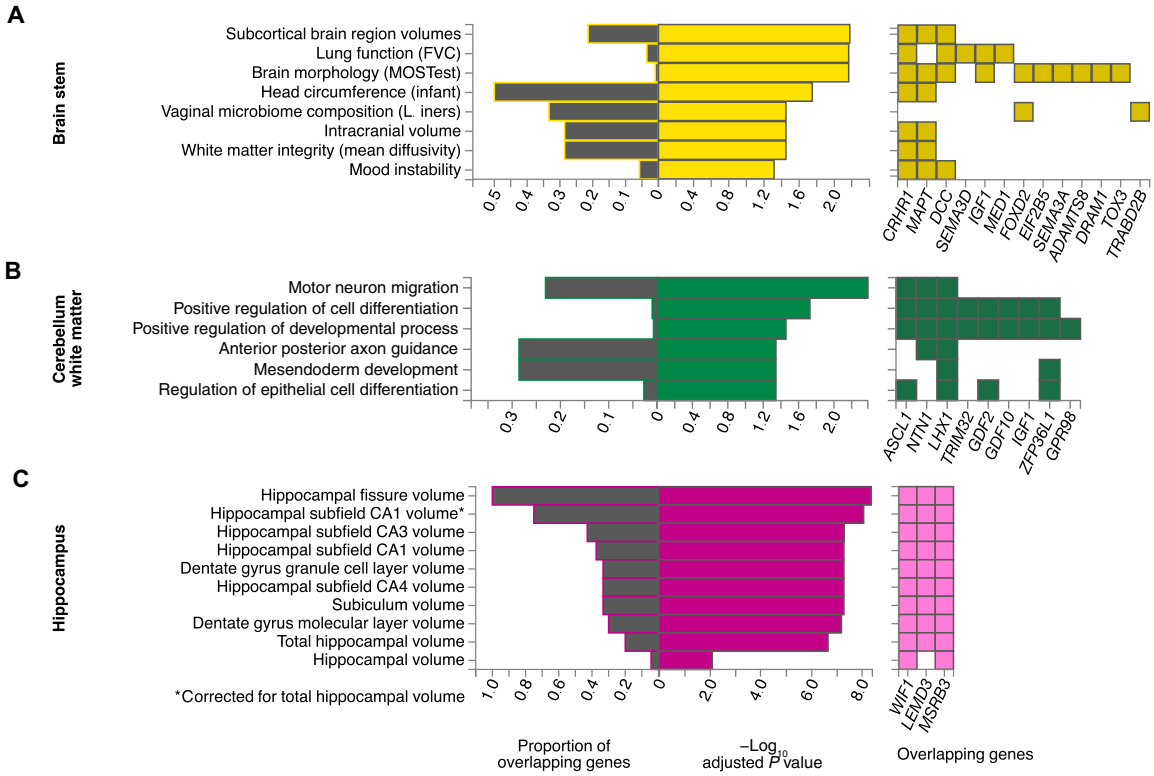

Fig. 5. Gene set enrichment results of selected brain structures. Significance of overrepresentation and overlap of prioritized genes with trait-associated gene sets from the GWAS catalog (**A** and **C**) and from GO biological processes (**B**) using hypergeometric tests. The figure displays results for selected brain structures, which stood out in the PCA (Fig. 3). All other structures can be found in Fig. 6 and in the Supplementary Materials (fig. S5). *P* values were corrected for multiple testing in each category by the Benjamini-Hochberg method.

assume that Winner's Curse (*48*) is an important explanation for this difference. However, the replication rate of the novel GWAS signals is still within the range observed in other studies on the genetics of brain structures (*9*).

To assess what can be expected as replication rate, we performed four age- and sex-stratified random splits of our discovery set into sample sizes of 80% (~15,000) and 20% (~4000) each and performed GWAS again for all brain structures in each of the four 80% samples. Applying the same significance threshold as in our original GWAS ($P < 1/22 * 5 \times 10^{-8}$), we replicated between 55.6 and 69.6% of all independent significant signals in all brain structures (mean ± SD = 62.9 ± 5.9%) at the nominal significance level ($P < 0.05$) and between 48.1 and 62.3% (mean ± SD = 56.5 ± 6.5%) at a 0.05 significance level after FDR correction in the respective 20% sample (table S19). In view of the fact that replication rates of GWASs usually are much lower than expected by power analysis (48% observed versus 91% expected), even after correction for Winner's Curse (48% versus 54%) (*48*), this simulation showed that our actual replication rate in a set of independent individuals was in keeping with the size of that set.

Robustness analysis

Because MRI measurements of the brain stem can be influenced by the height of the individual, we conducted the MOSTest analysis again with height as an additional covariate (fig. S10 and table S20). We replicated 35 of 37 independent significant SNPs at the Bonferroni-corrected genome-wide significance threshold ($P < 2.27 \times 10^{-9}$) and all 37 at the genome-wide significance threshold ($P < 5 \times 10^{-8}$). All of them were significant after FDR correction at the 0.05 threshold.

Outliers may emerge in any standardized neuroimaging data analysis pipeline. Therefore, we reanalyzed after removal of LBS outliers (see the Supplementary Materials). Small fluctuations in *P* values occurred with 10 of 148 associations showing a small increase, but all associations remained below the genome-wide significance threshold of 5×10^{-8} (table S7 and fig. S11). Similarly, the reanalysis of the CCA after outlier removal did not show any qualitative differences (fig. S12).

DISCUSSION

Examining the complex relationship among brain morphology, genetics, and neurological disorders is crucial for unravelling the underlying causes and enhancing our understanding of the anatomy of the human brain and diseases. The Laplace-Beltrami operator provides a useful spectral representation for describing shape characteristics. Adequately describing curvatures and being an informative topological fingerprint of the shape (*15*), the LBS captures more information compared to global shape quantities such as surface area or volume. Specifically, it captures local shape effects but still represents the whole form of an object because the respective eigenmodes are defined everywhere on the structure. Furthermore, the shape is described by a relatively small number of values, which simplifies data handling. Unlike other dimensionality reduction methods, such as PC analysis, it still preserves spatial interpretability. Also, it does

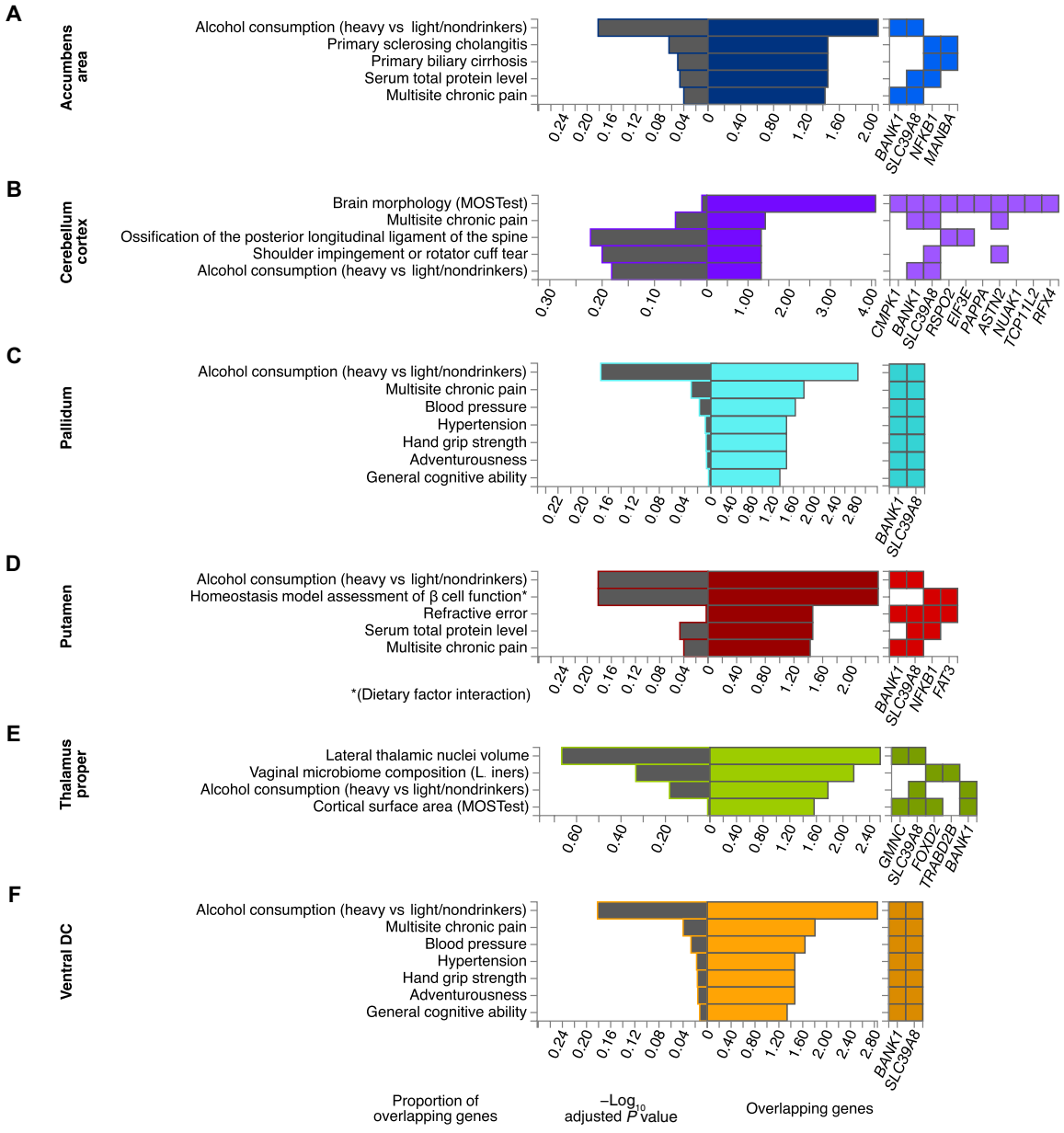

Fig. 6. Gene set enrichment results of brain structures with *BANK1* and *SLC39A8* as prioritized genes. Significance of overrepresentation and overlap of prioritized genes with trait-associated gene sets from the GWAS catalog using hypergeometric tests. *P* values were corrected for multiple testing in each category by the Benjamini-Hochberg method.

not depend on error-prone interindividual image registration, which is required by other methods. Using the LBS thus allowed us to specifically address the variation in shape independent of volume or surface area and to disentangle the genetics of morphology beyond those global properties. While the eigenmodes and their potential to explain shape-associated biological mechanisms have been recently explored (*22*), the eigenvalues were previously found to have considerable heritability in the case of subcortical brain structures and cerebellum (*6*). However, neither the genetic architecture at SNP level of the shape of brain structures nor possible relations to disease genetics have been investigated yet. Using state-of-the-art GWAS and the LBS (a set of eigenvalues) as a multidimensional phenotype, we have dissected the genetics of the shape of 22 brain structures in 19,862 White-British individuals from the UKB.

Overall, we identified 148 significant SNP associations that were independent in their respective GWAS. Because some SNPs were significantly associated with more than one brain structure, this resulted in 80 unique significant SNPs being independent across the 22 GWASs. Most of them, particularly the most significant ones, were detected in association with structures in the posterior fossa (brain stem and cerebellum). In contrast, we found no significant signal for the LBS of the amygdala. Because of the simple almond-like shape, crude measures like volume and surface area might already capture amygdala's shape well enough (Supplementary Materials,

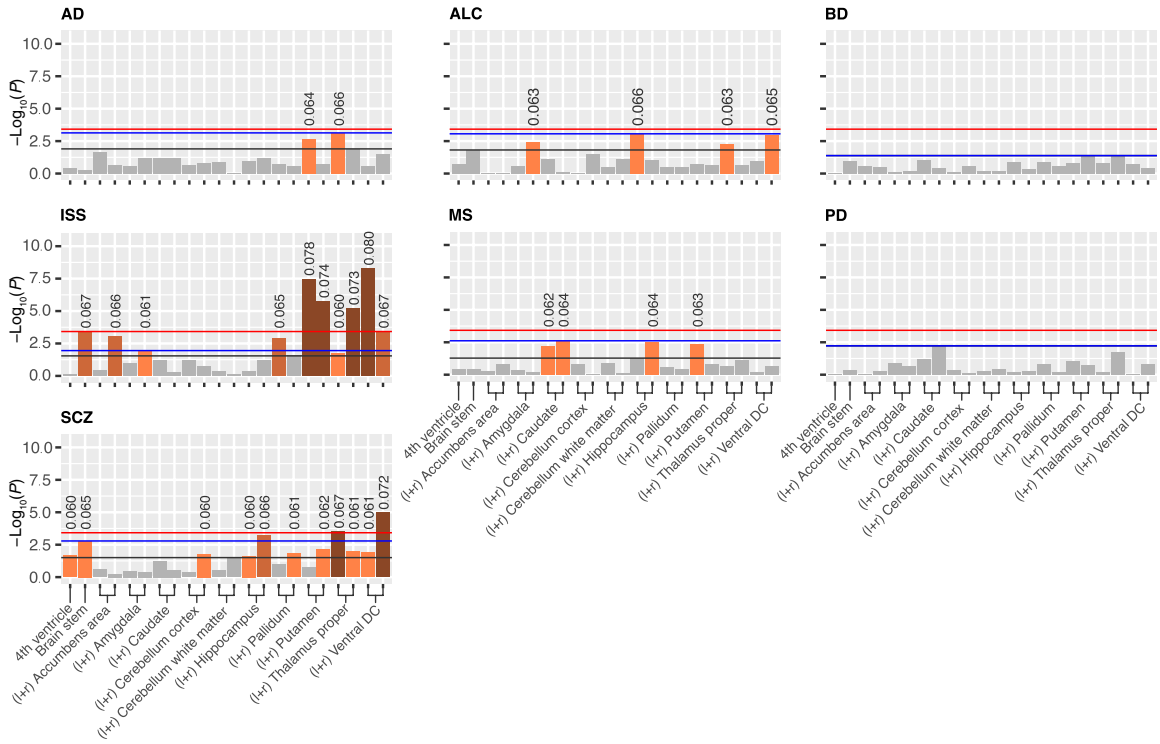

Fig. 7. *P* values of CCA results of various PRSs with different brain structures. Bar charts show the $-\log_{10}$-scaled *P* values of the correlations between PRSs and LBS of different brain structures at different significance thresholds: Bonferroni-corrected for 22 brain structures and 6 independent PRS (red line), FDR-corrected within each PRS (black line), and FDR-corrected within each PRS + Bonferroni-corrected for six independent PRS (blue line). Above significant *P* values, the correlation value is stated. For bilateral structures, the two results are displayed next to each other, with the left-side result ("l.") on the left.

table S21). This could possibly explain the lack of genetic signal in our study because we controlled for both volume and surface area.

Of those 80 SNPs, 37 have previously been reported as genome-wide significant in a large GWAS on subcortical volumes (*2*), while 4 were identified in a large GWAS meta-analysis on total brain volume (*1*). This overlap with volume-associated SNPs suggests pleiotropic effects of the respective gene loci, affecting both volume and shape characteristics independent of volume, while it is unlikely that pure volume associations were picked because we controlled for volume. Our hippocampus LBS GWAS, for instance, replicated 100% of all loci previously associated with hippocampal fissure size (*49*), which obviously influences hippocampal shape, while accounting for only 20% of the loci associated with total hippocampal volume (Fig. 5C).

Thirty-one of the 80 independent SNPs were not associated with any brain shape–related trait according to the GWAS catalog, neither by themselves nor by any variant in LD with them $(r^2 \geq 0.6)$, and 18 were not listed at all (table S1). This shows a substantial degree of novelty, that is, undiscovered genetic effects specific to the shape of brain structures, and supports the notion of SNPs affecting the development of form independent of growth.

Using a 15 times larger sample size, we were able to substantially refine the LBS SNP heritability estimates of subcortical brain structures, including the cerebellum, previously provided by Ge *et al.* (*6*) ($N = 1320$). While their estimates ranged from 0.005 to 0.5, some being nonsignificant because of large standard errors of 0.12 to 0.21, our estimates were between 0.1 and 0.3, all being significant with much lower standard errors (≤0.005). Statistical tests implied that our heritability estimates did not differ significantly from those of Ge *et al.* This was likely due to the much larger standard errors of their estimates but may also be a consequence of the younger age span in their cohort (18 to 35 years). Overall, we achieved results with higher statistical significance corresponding to our larger sample size and also likely due to our additional control for total brain volume, the respective local surface area, and MRI scan quality. The refined estimates were approximately equal to the SNP heritability of volumetric traits of subcortical structures that Hibar *et al.* (*3*) derived from similar sample sizes or even larger as in the case of caudate, hippocampus, and putamen, for which they derived an SNP heritability of about 0.11 with 95% CI < 0.16 each, while we found values of 0.29, 0.20, and 0.18, respectively.

Bilateral structures showed similar genetic architecture of LBS (Fig. 3), which could be expected because of their symmetry. Moreover, genetic architecture was also shared between structures, as suggested by their adjacent positions, e.g., in the case of the basal ganglia. The two noticeably frequently shared variants rs13107325 and rs12146713 on *SLC39A8* and *NUAK1*, respectively, seem to affect brain shape globally as they have recently been associated with the structural connectome (*40*). While *SLC39A8*, as a brain metal transporter, is involved in several brain and neurodevelopmental traits (see below), *NUAK1* is also known to regulate axon branching by controlling mitochondrial distribution (*50*). The genetic associations of cerebellum and brain stem LBS were more different. The brain stem stood out because of a high number of specific association signals. These included the ExNS variant rs1687225 in *VWA5B2*, the gene of von Willebrand factor A domain containing protein 5B2. This

Table 2. Heritability estimates of different brain structures. Heritability estimates are presented for single brain structures (h^2) and for combined regions (h^2 combined) as well as their standard errors (SE and SE combined). Here, numbers in bold are significant after Bonferroni correction for 22 brain structures. For comparison, the estimates from Ge *et al.* (*6*) are listed in the last two columns. Italic numbers are nominally significant, and bold ones are significant after false discovery rate correction in (*6*).

Brain structure	h^2	SE	h^2 combined	SE combined	h^2 Ge2016	SE Ge2016
4th ventricle	**0.169**	3.0×10^{-3}	**0.169**	3.0×10^{-3}	0.005	0.208
Left accumbens area	**0.134**	2.8×10^{-3}	**0.116**	1.9×10^{-3}	*0.237*	0.135
Right accumbens area	**0.095**	2.4×10^{-3}				
Left amygdala	**0.105**	2.5×10^{-3}	**0.118**	1.8×10^{-3}	–	–
Right amygdala	**0.134**	2.8×10^{-3}				
Left caudate	**0.296**	1.9×10^{-3}	**0.285**	1.4×10^{-3}	***0.499***	0.188
Right caudate	**0.273**	2.0×10^{-3}				
Brain stem	**0.282**	5.4×10^{-3}	**0.198**	1.5×10^{-3}	***0.452***	0.192
Left cerebellum cortex	**0.186**	2.9×10^{-3}				
Right cerebellum cortex	**0.194**	2.8×10^{-3}				
Left cerebellum white matter	**0.195**	2.6×10^{-3}				
Right cerebellum white matter	**0.148**	2.6×10^{-3}				
Left hippocampus	**0.187**	2.6×10^{-3}	**0.199**	1.9×10^{-3}	***0.347***	0.169
Right hippocampus	**0.210**	2.7×10^{-3}				
Left pallidum	**0.124**	2.9×10^{-3}	**0.122**	2.0×10^{-3}	0.061	0.117
Right pallidum	**0.120**	2.8×10^{-3}				
Left putamen	**0.158**	2.7×10^{-3}	**0.183**	1.9×10^{-3}	***0.413***	0.148
Right putamen	**0.210**	2.8×10^{-3}				
Left thalamus proper	**0.134**	2.7×10^{-3}	**0.132**	1.9×10^{-3}	0.086	0.143
Right thalamus proper	**0.130**	2.7×10^{-3}				
Left ventral DC	**0.122**	2.7×10^{-3}	**0.146**	2.1×10^{-3}	–	–
Right ventral DC	**0.169**	3.2×10^{-3}				

missense variant belongs to the 3% most deleterious variants (according to the CADD score) and was also an independent brain cis-eQTL of *VWA5B2* according to GTEx (version 8). Proxy variants of rs1687225 have been reported as being associated with brain morphology (*2*), cortical thickness (*51*), and educational achievement (*52*).

An extended genomic risk locus on chromosome 17 with lead SNP rs568589031 was also rather specific for the brain stem. ExNS variant rs17651549 at this locus had the highest CADD score (26.8) of all variants in LD with any of the independent significant SNPs. It affects *MAPT*, which was among the most significant signals in MAGMA gene-based analysis of the brain stem LBS. However, this locus contains multiple protein-coding genes with several brain cis-eQTLs affecting them and other genes in the region (table S6). The analysis of this large locus is highly challenging. The locus has previously been mapped to brain morphology (*2*) and several neurodegenerative diseases such as progressive supranuclear palsy, corticobasal degeneration, frontotemporal dementia, PD, and AD (*42*, *43*, *53*–*62*). Moreover, variations in cortical morphology have recently been linked to *APOE ε4* and *MAPT* in young healthy adults (*63*). There is also evidence of brain stem deformations in early stages of AD manifesting as variations in the midbrain (*64*), decreased locus coeruleus (part of the brain stem) volume preceding neuronal loss (*65*), and neurofibrillary tangle–related neurodegeneration in the brain stem potentially causing neuropsychiatric symptoms (*66*). While patients with diagnosed neurodegeneration were excluded from our study, the possibility remains that preclinical stages might potentially mediate the genetic relation between shape and the *MAPT* locus. However, neither gene enrichment analysis (Figs. 4 to 6) nor CCA (Fig. 7), as an enrichment analysis independent of candidate genes, did provide evidence for a significant correlation between the genetics or phenotype of brain stem LBS and the genetics, respectively the PRS, of neurodegeneration such as AD.

At this locus, significant ExNS SNPs with high CADD scores were also found in *SPPL2C*, *KANSL1*, and *CRHR1*, which showed the strongest signal in the MAGMA analysis (Table 1 and Fig. 4A). Loss-of-function variants of *KANSL1* are known for causing autosomal-dominant Koolen-de-Vries syndrome (MIM no. 610443) which is

characterized by intellectual disability and structural brain abnormalities (*67*). *SPPL2C* is the gene of signal peptide peptidase–like 2C and has previously been highlighted in a GWAS on total brain volume because of a relatively large number of ExNS variants (*1*). However, we controlled for volume in our GWAS on brain shape. A recent study found that *CRHR1*, which encodes a receptor for the corticotropin-releasing hormone CRH, moderates brain volume differences, possibly through its stress response function, which in return mediates the relationship between urban environmental exposure and affective symptoms (*68*). In particular, in the context of *CRHR1*, lower brain volume was observed in relation to stronger affective symptoms and greater urban environment exposure. Variants of *CRHR1* have further been associated with alcohol (*69*) and heavy alcohol consumption following stressful life (*70*). Even light alcohol consumption has recently been related to changes in brain structure (*71*). Genes associated with the LBS of several other brain structures were enriched in gene sets associated with alcohol consumption (Fig. 6). Thus, alcohol consumption may be a potential mediator of their effect on brain shape. However, we would like to note that the enrichment was driven by one locus.

That locus on chromosome 4 with lead SNP rs13107325, an ExNS variant of *SLC39A8*, not only appeared to be significant in most brain structures (15 structures including the brain stem, albeit with a subthreshold significance) but also revealed the overall strongest signal across all the GWASs in left cerebellum white matter. This locus, especially the lead SNP, has a pleiotropic effect. Besides alcohol consumption (*72*), it has been linked to SCZ (*33*–*35*), Crohn's disease (*36*), blood pressure and cardiovascular disease risk (*37*), and several brain imaging phenotypes (*9*). The cerebellothalamic and cerebellar-basal ganglia connectivity dysfunction hypothesis in individuals with SCZ is supported by the significant and prominent occurrence of rs13107325 in precisely these regions (*73*, *74*). SCZ is known to be associated with abnormalities of subcortical brain structures (*75*–*77*). Clinical features of SCZ might be due to aberration of dendritic spine density (*78*). A knockin mouse model of rs13107325 points to an increased risk of SCZ by regulating zinc transport and dendritic spine density and subtle effects on cortical development because of this variant (*79*). A recent gene mapping study concluded strong evidence for pleiotropic genes associated with SCZ and brain structure with evidence of brain variation causing SCZ (*80*).

SCZ shows substantial genetic correlation (0.68) with BD (*81*), which was also evident in the correlation (0.37) between their PRSs. However, BD seems to have less relation to brain morphology. Madre *et al.* (*82*) investigated cortical morphology in individuals with SCZ and BD and reported shared volume and thickness deficits, while abnormalities of geometry and curvature were specific to SCZ. Also, Stauffer *et al.* (*80*) reported the association of MRI metrics to be weaker with BD genetics than with SCZ genetics. Our results are in line with these findings as CCA revealed correlation of the LBS of several brain structures only with the SCZ-PRS, while there was no correlation with BD-PRS (Fig. 7). This result suggests that LBS may therefore be sensitive to SCZ-specific brain shape variations and thus potentially helpful for the differential diagnosis of psychosis.

CCA also revealed highly significant links between the LBS of multiple brain structures and the PRS of ISS in our healthy cohort (Fig. 7). In line with the high correlation between ISS-PRS and HT-PRS, CCA produced a very similar result for the HT-PRS (fig. S13). HT is associated with white matter hyperintensities and cognitive dysfunction in elderly patients and is a major risk factor for ISS (*83*). A recent study showed that morphological changes in the basal ganglia and thalamus already occurring in midlife are associated with blood pressure and, therefore, might be better markers of early HT than volume aberrations (*84*). Our CCA results were especially significant in these brain regions, which in turn support the suggestion of using brain morphology or shape as an early biomarker of HT.

Limitations of our study include the lack of effect sizes (β values) in our multivariate results, which impedes the use of conventional post-GWAS tools such as genetic correlation and Mendelian randomization analyses. Instead, we explored the relationship to genetics of other traits by performing CCA between LBSs and PRSs. This was limited by the predictive power of each PRS. Furthermore, we could not establish the causal relationship between genetic variation in brain morphology and a particular trait or disease. Restricting our study to healthy individuals may additionally have yielded lower effect sizes and potentially false negative correlations when performing disease-related analyses. Also, we did not yet address the cortex, a brain structure that relates to a plentitude of neurophysiological and neuropsychiatric phenomena. A follow-up study on the shape of the cortex and its subregions may provide further insights.

In summary, we have delineated the genetic architecture of brain shapes beyond global measurements such as volume and surface area by using the LBS as a mathematical shape descriptor. In our multivariate GWAS on a large healthy cohort of the UKB, we identified 80 unique independent SNPs with brain stem showing a distinctly high number of specific association signals, which included the *MAPT* locus implicated in neurodegenerative diseases. The shapes of most brain structures were significantly associated with the pleiotropic variant rs13107325, a known risk factor for SCZ. We further identified significant correlations between brain shape and PRSs of SCZ, HT, and ISS, suggesting the potential use of the LBS as an early disease biomarker. As such, the LBS expands the set of tools for investigating brain shapes, holding implications for early detection of a wide spectrum of traits, and warrants further research in disease-specific cohorts.

MATERIALS AND METHODS

UKB data and sample filtering

Data were retrieved from the official source of the UKB (application number 41655) and provided as a DataLad dataset, a research data management solution providing data versioning, data transport, and provenance capture (*85*). UKB has ethical approval from the Northwest Multi-Centre Research Ethics Committee (REC reference: 21/NW/0157), and all participants have provided written informed consent. A total of 487,409 genotyped samples was available (v3 imputed on Haplotype Reference Consortium and UK10K haplotype data, aligned to the + strand of the reference and GRCh37 coordinates, released in 2018, data field 22828). We kept only self-reported White-British individuals for data homogeneity according to data field 21000, resulting in 430,560 individuals. After genetic QC (see below), there were 393,913 unrelated samples left. A total of 30,080 of them had structural MRI data (T1) on which we calculated the LBS (see below) of 22 brain structures (Fig. 1) of 24,834 individuals without mental or behavioral disorders (ICD index F) or diseases of the nervous system (ICD index G) according to the International Statistical Classification of Diseases and Related Health Problems 10th revision (ICD-10).

We created age- and sex-stratified discovery and replication samples by splitting the data into two subsets comprising 80 and 20% of the individuals, respectively. Excluding samples without total brain volume data (see below), our final dataset for our discovery GWAS contained 19,862 individuals, 9435 male and 10,427 female, ranging in age between 46.0 and 81.7 years with a mean ± SD of 64.3 ± 7.4 years (female: 63.6 ± 7.3; male: 65.0 ± 7.5).

QC of genetic data

We conducted QC using Plink2 (version: 26 August 2021) whenever possible and Plink (version 1.9, 6 June 2021) for some missing functionalities on all self-reported White-British individuals and their imputed genotype data. For this purpose, the data records were first converted from BGEN to binary Plink2 format, and only SNPs were kept for further analyses. As recommended by UKB (*86*), we removed variants with an imputation score less than 0.3, and following Mills *et al.* (*87*), we excluded all variants with a call rate less than 0.95, a minor allele frequency of less than 0.01, and a Hardy-Weinberg equilibrium exact test P value below 1×10^{-6}. As recommended by Plink2, we used the mid-P adjustment to reduce the filter's tendency to retain variants with missing data (*88*) and the keep-fewhet modifier. We also removed samples with a mismatch between self-reported and genetically inferred sex, with genotype missingness of more than 0.05, and all heterozygosity outliers (±3 SD). Moreover, using a kinship coefficient of 0.088 and the king-cutoff command, we randomly excluded one from each pair of individuals related to greater than or equal to second degree. Only autosomal SNPs were examined. In total, 8,105,763 SNPs remained after QC. We calculated the first 10 PCs from them, which were included as covariates in the GWASs.

Image data processing

First, we segmented anatomical structures from all available T1 MRI brain scans with FreeSurfer version 7.2.0 (*89*–*93*). Second, we created triangular meshes for all structures of interest. Last, we computed compact shape representations for all structures using the BrainPrint Python package (*21*) (see below). To account for the quality of the MRI scans, we computed the Euler number with FreeSurfer. This represents the total defect index and is a measurement of the number of holes in the calculated surface.

Multidimensional shape descriptor

A shape, parameterized as a Riemannian manifold M, may be described by its intrinsic geometric information, which can be obtained by solving the Helmholtz equation on that manifold

$$\Delta f = -\lambda f$$

where Δ is the Laplace-Beltrami operator, a generalization of the Laplace operator in Euclidean space; and f is a real-valued function, with $f \in C^2$, defined on M. The solutions (f_i, λ_i) represent the spatial part of the wave equation with eigenfunctions f_i and eigenvalues λ_i where $\sqrt{\lambda_i}$ can be interpreted as the natural frequencies. The set of all eigenvalues is called the spectrum of an operator. The LBS or ShapeDNA (*13*) is accordingly defined as the beginning subsequence of the increasingly ordered spectrum of the Laplace-Beltrami operator solved on a Riemannian manifold

$$\{\lambda_1, \ \ldots, \lambda_N\} \ \text{ with } \ 0 \le \lambda_i \le \lambda_j \quad \forall i < j$$

The LBS was computed with the BrainPrint package (*21*) based on the FreeSurfer output. For each individual, we calculated the first, i.e., the smallest, 50 eigenvalues of each brain structure as done in (*6*). Because the first eigenvalue is always zero, since each object is a closed surface without a boundary, we used only the next 49 values in our analyses. Each eigenvalue $\lambda_{i,m}$ was further normalized to volume V_i of each brain structure i. The volume and surface area were calculated by BrainPrint. Afterward, $\lambda_{i,m}$ was divided by its position m in the ordered spectrum to balance out the higher eigenvalues, which more likely represent noise (*6*, *13*, *21*)

$$\bar{\lambda}_{i,m} = \frac{1}{m}\left(\lambda_{i,m} \cdot V_i^{\frac{2}{3}}\right), \forall i \in \{1, \ \ldots, 22\}, m \in \{2, \ \ldots, 50\}$$

In the end, we analyzed 22 brain structures as provided by FreeSurfer: 4th ventricle, brain stem, accumbens area (left and right), amygdala (left and right), caudate (left and right), cerebellum cortex (left and right), cerebellum white matter (left and right), hippocampus (left and right), pallidum (left and right), putamen (left and right), thalamus proper (left and right), and ventral DC (left and right). By that, we handled the normalized and reweighted LBS $\{\bar{\lambda}_{i,2}, \ \ldots, \bar{\lambda}_{i,50}\}$ for each brain structure i as a 49-dimensional quantitative trait.

Multivariate genome-wide association analysis

For our multivariate GWAS, we used the MOSTest tool, a multivariate omnibus test, which handles big data efficiently and accounts for the correlation among the phenotypes to increase statistical power (*2*). Because the eigenvalues are not independent in general {Pearson correlation range: [0.285;0.998]; mean ± SD = 0.93 ± 0.06; figs. S14 to S16}, we conducted, for each brain structure i, a multivariate GWAS on the 49 volume-normalized and scaled eigenvalues $\bar{\lambda}_{i,m}, m \in \{2, \ \ldots, 50\}$, treating each $\bar{\lambda}_{i,m}$ as a single quantitative phenotype. For that, we first calculated residuals of the multidimensional phenotype to control for potential covariates as recommended by MOSTest, i.e., we regressed each $\bar{\lambda}_{i,m}$ on age, age^2, sex, first 10 genetic PCs, Euler number, surface area of each brain structure i, and the total brain volume. The latter was calculated as the sum of the volume of ventricular cerebrospinal fluid (data field 25004) and the gray and white matter volume (data field 25010) in line with Jansen *et al.* (*1*). Normalizing the LBS to volume as described above and regressing out total brain volume and surface area of each brain structure assured that we studied the shape and not linear size effects. We defined the residualized eigenvalues $\tilde{\lambda}_{i,m}$ as the sum of the estimated intercept and the residuals of its linear regression. After adjusting for covariates, the range of absolute correlations between all $\tilde{\lambda}_{i,m}$ values was quite high {Pearson correlation range: [0;0.978]; mean ± SD = 0.65 ± 0.18; figs. S14 to S16}. We further inspected the relation of each $\tilde{\lambda}_{i,m}$ to volume and surface area by calculating their Pearson correlations. There was, as expected, no correlation with surface area and a low correlation with volume (mean ± SD = 0.27 ± 0.08) (fig. S17). The effect was small except for the eigenvalues of caudate, which showed mean correlations of 0.50 (left) and 0.46 (right) both with an SD of 0.05, likely relating to the long C-shaped form of that structure and by the fact that volume normalization (i.e., multiplication with $V_i^{\frac{2}{3}}$; see above) excludes the pure size effects but not a real difference in shape. Including volume as an additional covariate in the MOSTest analysis produced nevertheless similar results (table S22).

All $\tilde{\lambda}_{i,m}$ values were then passed to MOSTest, which first performs a rank-based inverse-normal transformation (INT) to obtain normally distributed data. This is followed by a standard additive univariate GWAS for each $\tilde{\lambda}_{i,m}$, resulting in z-scores for each SNP

and $\widetilde{\lambda}_{i,m}$. This procedure is repeated with once-permuted genotypes, preserving phenotype correlation. The MOSTest test statistic for an SNP is then calculated as the Mahalanobis norm of the nonpermuted z-scores of that SNP and the correlation matrix R of the z-scores from once-permuted genotypes of all eigenvalues. The P value of the multivariate test statistic is then calculated from a cumulative distribution function of a fitted gamma distribution, which eliminates the need for a multiple testing correction of 49 univariate GWASs and therefore allows to determine the significance of SNPs with a P value below the standard genome-wide threshold of 5×10^{-8}. We further confirmed that MOSTest controlled the type I error sufficiently by plotting P values from empirical distributions of the test statistic and from fitted gamma functions under the null hypothesis as calculated by permutating the phenotype-genotype assignments (figs. S18 to S39).

Identification of genomic loci and functional annotations

For functional annotations, we used the web-based platform FUMA (version 1.5.6) (*28*). We used default settings to determine genomic risk loci. First, independent significant SNPs were identified as the ones with a P value equal to or smaller than 2.27×10^{-9} (Bonferroni correction for 22 brain structures: $1/22 * 5 \times 10^{-8} = 2.27 \times 10^{-9}$) and LD with other such SNPs in its vicinity of $r^2 < 0.6$. These SNPs and those in LD with them $(r^2 \geq 0.6)$ were defined as candidate SNPs and used in subsequent analyses. LD computation was based on the European population within the 1000 Genomes reference panel (phase 3) (*94*). Those with $r^2 < 0.1$ were classified as lead SNPs among the independent significant SNPs. Independent significant SNPs with $r^2 \geq 0.1$ or with a gap of less than 250 kb between their respective LD blocks (all SNPs in LD $r^2 \geq 0.6$ with them) were merged into one genomic risk locus. Therefore, a genomic risk locus can contain multiple independent significant SNPs.

Candidate SNPs were used for functional annotations. Positional annotation was performed with ANNOVAR (*29*). Furthermore, SNPs were annotated with CADD scores, RegulomeDB scores, and 15-core chromatin states. The major histocompatibility region was excluded from all annotations. For eQTL mapping, we checked several available databases containing relevant information, i.e., PsychENCODE eQTLs, CommInMind Consortium, BRAINEAC, and GTEx v8 Brain, and extracted all significant SNP-gene pairs with an FDR [Benjamini-Hochberg procedure (*46*)]–controlled P value < 0.05 within the respective database.

Gene mapping and gene enrichment analysis

For gene prioritization, we used PoPS (version 0.2) (*44*), a tool that assigns polygenic priority scores to each gene by fitting their MAGMA z-scores to trait-relevant gene features extracted from cell type–specific gene expression, biological pathways, and protein-protein interactions. We calculated these z-scores using MAGMA (version 1.10) (*41*) by first annotating SNPs to 18,383 protein-coding genes within a 0-kb window and afterward performing gene analysis using the SNP-wise mean model and the European population of 1000 Genomes as a reference dataset for every brain structure. We then ran PoPS on our MAGMA scores using default settings and all available 57,543 gene features. Gene annotation and location files, as well as gene features, were taken from www.finucanelab.org/data.

Lead SNPs, as defined by FUMA (see above), were mapped to genes within a 500-kb window up- and downstream. We first selected the four genes with the highest PoPS score in each locus. Second, because it was shown that PoPS works best when combined with orthogonal methods like Nearest Gene, we mapped each lead SNP to the two closest genes. After assigning a rank to each gene by both methods and averaging the two ranks, we reranked the genes and lastly prioritized all genes with an average rank ≤2 for each independent significant SNP.

The prioritized genes were given as input to the FUMAs Gene2Func tool. Genes of brain structures present in both hemispheres were joined in each analysis. We used all protein-coding genes of Ensembl version 110. Hypergeometric tests analyzed the overrepresentation of mapped genes in precalculated gene sets followed by an FDR control (Benjamini-Hochberg, $P < 0.05$) within each category.

CCA with PRS

For the CCA, we extracted PRSs of six brain shape–related traits and disorders and that of one trait that stood out from the FUMA gene set results. Six PRSs were taken from the UKB, which have exclusively been trained on external datasets: AD (data field 26206), BD (data field 26214), ISS (data field 26248), MS (data field 26254), PD (data field 26260), and SCZ (data field 26275). Furthermore, we calculated the PRS for ALC based on the score definition from the PGScatalog (*95*) [PGS002738 (*96*)]. UKB data were not used for evaluating this last score but for one GWAS in the discovery meta-analysis of the ALC study. The data was available for 19,850 samples. Each PRS was first linearly regressed on age, age^2, sex, first 10 genetic PCs, and total brain volume. The residuals were added to the fitted intercept. Second, a rank-based INT was applied to those PRSs. The partial correlation between the PRSs was calculated as a Pearson correlation. We used the residualized eigenvalues $\widetilde{\lambda}_{i,m}$ as they were used as input for MOSTest for each brain structure and applied a rank-based INT.

For each pair of PRS and brain structure, we conducted a CCA using the cca() function within the "yacca" R-package (version 1.4-2). CCA finds a linear combination of all eigenvalues, a so-called canonical variable, which correlates maximally with the PRS. All resulting P values of the correlations were adjusted for multiple testing using FDR. Afterward, we applied an additional Bonferroni correction for six effective PRSs, which we consider as the two-level correction. For comparison, we also calculated the Bonferroni correction for 22 * 6 tests. All adjustments were made to the 0.05 significance threshold.

Furthermore, in each CCA, we investigated the loadings, i.e., the correlations of all eigenvalues with their canonical variable, which describe the direction and strength of the impact of each eigenvalue on the risk score. Out of those, we calculated the mean loading and the number of negative/positive loadings of all eigenvalues in each brain structure and PRS. If at least 90% of all loadings had the same direction, we deemed that as a common direction of effects. Hierarchical clusters were computed on the distances of mean loadings among brain structures and PRSs using the complete linkage method (fig. S8).

SNP-based heritability

Ge *et al.* investigated the heritability of neuroanatomical shape using the LBS. For estimating its SNP heritability, they proposed a multidimensional approach where they summed the univariate heritability h_m^2 of the eigenvalues, each weighted by γ_m, the relative size of its phenotypic variance

$$h^2 = \sum_m \gamma_m h_m^2, \text{with } \gamma_m = \frac{\sigma_{P_m}^2}{\sum_k \sigma_{P_k}^2}$$

and $\sigma^2_{P_m}$ being the phenotypic variance of trait m. The univariate heritabilities of the 49 eigenvalues were derived using SCORE. For combined structures, we derived the multidimensional heritability from the union set of eigenvalues. When applying SCORE, we proceeded as with the GWAS described above using volume-normalized and reweighted eigenvalues and the same set of covariates. The phenotypic variance was also computed using the residualized eigenvalues $\tilde{\lambda}_{i,m}$. We further calculated the P value of each heritability using the Wald test statistics, which is distributed as

$$\left(\frac{h^2}{\mathrm{SE}(h^2)}\right)^2 \sim \frac{1}{2}\chi_0^2 + \frac{1}{2}\chi_1^2$$

with χ_0^2 being the point mass at 0 and χ_1^2 being the chi-squared distribution with one degree of freedom because the null hypothesis $H_0: h^2 = 0$ lies on the boundary of a constrained parameter space ($h^2 \geq 0$) (*97*). The standard error (SE) of each multidimensional heritability was calculated using Bienayme's identity for the variance of a sum and the univariate estimates from SCORE as follows

$$\mathrm{SE}(h^2) = \sqrt{\sum\nolimits_m \gamma_m^2 \mathrm{SE}(h_m^2)^2}$$

For testing the difference between heritability values in each combined brain structure, we used the Wald test statistics distributed as

$$\left(\frac{h^2 - h^2_{\mathrm{Ge}}}{\mathrm{SE}(h^2 - h^2_{\mathrm{Ge}})}\right)^2 \sim \chi_1^2$$

with

$$\mathrm{SE}(h^2 - h^2_{\mathrm{Ge}})^2 = \mathrm{SE}(h^2)^2 + \mathrm{SE}(h^2_{\mathrm{Ge}})^2 - \mathrm{SE}(h^2)\mathrm{SE}(h^2_{\mathrm{Ge}})\mathrm{cor}(h^2, h^2_{\mathrm{Ge}})$$

Because $\mathrm{SE}(h^2)$ is small in comparison to $\mathrm{SE}(h^2_{\mathrm{Ge}})$, we can approximate $\mathrm{SE}(h^2 - h^2_{\mathrm{Ge}})^2$ by just $\mathrm{SE}(h^2_{\mathrm{Ge}})^2$.

Replication

Replication analysis was conducted on the 20% sample (see above). This encompassed 4963 individuals, of which 4961 (2605 female) had data of total brain volume available, ranging in age from 45.2 to 81.8 years (age mean ± SD = 64.2 ± 7.4; female: 63.6 ± 7.2; male: 64.9 ± 7.6). In these 4961 individuals, we performed MOSTest analyses of each brain structure using all SNPs that passed QC and the same procedure and set of covariates as in the discovery analysis. For each brain structure, we only investigated those variants of the 80 independent SNPs that had shown Bonferroni-corrected genome-wide significance in the respective discovery GWAS. FDR correction was applied to these P values for each brain structure separately.

To find a range for the expected replication rate, we subdivided the original discovery dataset (19,862 individuals) four times into a set of 80% (~15,000 individuals) for discovery and a set of 20% (~4000 individuals) for replication. The splits corresponded to the relative size of our actual replication set and were done randomly while preserving equal age and sex distribution in discovery and replication sets. The GWAS on the 80% sets and the replication were done following the same methods, covariates, and significance threshold as before. Replication rates were calculated on the set of significant independent variants of each split and brain structure, obtained by Plink2 (version: 24 June 2024) by using the same clumping parameters as given to FUMA before (see the "Identification of genomic loci and functional annotations" section).

Supplementary Materials

The PDF file includes:

Supplementary Text
Figs. S1 to S39
Legends for tables S1 to S22
References

Other Supplementary Material for this manuscript includes the following:

Tables S1 to S22

REFERENCES AND NOTES

1. P. R. Jansen, M. Nagel, K. Watanabe, Y. Wei, J. E. Savage, C. A. De Leeuw, M. P. Van Den Heuvel, S. Van Der Sluis, D. Posthuma, Genome-wide meta-analysis of brain volume identifies genomic loci and genes shared with intelligence. *Nat. Commun.* **11**, 5606 (2020).
2. D. van Der Meer, O. Frei, T. Kaufmann, A. A. Shadrin, A. Devor, O. B. Smeland, W. K. Thompson, C. C. Fan, D. Holland, L. T. Westlye, O. A. Andreassen, A. M. Dale, Understanding the genetic determinants of the brain with MOSTest. *Nat. Commun.* **11**, 3512 (2020).
3. D. P. Hibar, J. L. Stein, M. E. Renteria, A. Arias-Vasquez, S. Desrivières, N. Jahanshad, R. Toro, K. Wittfeld, L. Abramovic, M. Andersson, B. S. Aribisala, N. J. Armstrong, M. Bernard, M. M. Bohlken, M. P. Boks, J. Bralten, A. A. Brown, M. M. Chakravarty, Q. Chen, C. R. K. Ching, G. Cuellar-Partida, A. den Braber, S. Giddaluru, A. L. Goldman, O. Grimm, T. Guadalupe, J. Hass, G. Woldehawariat, A. J. Holmes, M. Hoogman, D. Janowitz, T. Jia, S. Kim, M. Klein, B. Kraemer, P. H. Lee, L. M. Olde Loohuis, M. Luciano, C. Macare, K. A. Mather, M. Mattheisen, Y. Milaneschi, K. Nho, M. Papmeyer, A. Ramasamy, S. L. Risacher, R. Roiz-Santiañez, E. J. Rose, A. Salami, P. G. Sämann, L. Schmaal, A. J. Schork, J. Shin, L. T. Strike, A. Teumer, M. M. J. van Donkelaar, K. R. van Eijk, R. K. Walters, L. T. Westlye, C. D. Whelan, A. M. Winkler, M. P. Zwiers, S. Alhusaini, L. Athanasiu, S. Ehrlich, M. M. H. Hakobjan, C. B. Hartberg, U. K. Haukvik, A. J. G. A. M. Heister, D. Hoehn, D. Kasperaviciute, D. C. M. Liewald, L. M. Lopez, R. R. R. Makkinje, M. Matarin, M. A. M. Naber, D. R. McKay, M. Needham, A. C. Nugent, B. Pütz, N. A. Royle, L. Shen, E. Sprooten, D. Trabzuni, S. S. L. van der Marel, K. J. E. van Hulzen, E. Walton, C. Wolf, L. Almasy, D. Ames, S. Arepalli, A. A. Assareh, M. E. Bastin, H. Brodaty, K. B. Bulayeva, M. A. Carless, S. Cichon, A. Corvin, J. E. Curran, M. Czisch, G. I. de Zubicaray, A. Dillman, R. Duggirala, T. D. Dyer, S. Erk, I. O. Fedko, L. Ferrucci, T. M. Foroud, P. T. Fox, M. Fukunaga, J. R. Gibbs, H. H. H. Göring, R. C. Green, S. Guelfi, N. K. Hansell, C. A. Hartman, K. Hegenscheid, A. Heinz, D. G. Hernandez, D. J. Heslenfeld, P. J. Hoekstra, F. Holsboer, G. Homuth, J.-J. Hottenga, M. Ikeda, C. R. Jack, M. Jenkinson, R. Johnson, R. Kanai, M. Keil, J. W. Kent, P. Kochunov, J. B. Kwok, S. M. Lawrie, X. Liu, D. L. Longo, K. L. McMahon, E. Meisenzahl, I. Melle, S. Mohnke, G. W. Montgomery, J. C. Mostert, T. W. Mühleisen, M. A. Nalls, T. E. Nichols, L. G. Nilsson, M. M. Nöthen, K. Ohi, R. L. Olvera, R. Perez-Iglesias, G. B. Pike, S. G. Potkin, I. Reinvang, S. Reppermund, M. Rietschel, N. Romanczuk-Seiferth, G. D. Rosen, D. Rujescu, K. Schnell, P. R. Schofield, C. Smith, V. M. Steen, J. E. Sussmann, A. Thalamuthu, A. W. Toga, B. J. Traynor, J. Troncoso, J. A. Turner, M. C. Valdés Hernández, D. van't Ent, M. van der Brug, N. J. A. van der Wee, M.-J. van Tol, D. J. Veltman, T. H. Wassink, E. Westman, R. H. Zielke, A. B. Zonderman, D. G. Ashbrook, R. Hager, L. Lu, F. J. McMahon, D. W. Morris, R. W. Williams, H. G. Brunner, R. L. Buckner, J. K. Buitelaar, W. Cahn, V. D. Calhoun, G. L. Cavalleri, B. Crespo-Facorro, A. M. Dale, G. E. Davies, N. Delanty, C. Depondt, S. Djurovic, W. C. Drevets, T. Espeseth, R. L. Gollub, B.-C. Ho, W. Hoffmann, N. Hosten, R. S. Kahn, S. Le Hellard, A. Meyer-Lindenberg, B. Müller-Myhsok, M. Nauck, L. Nyberg, M. Pandolfo, B. W. J. H. Penninx, J. L. Roffman, S. M. Sisodiya, J. W. Smoller, H. van Bokhoven, N. E. M. van Haren, H. Völzke, H. Walter, M. W. Weiner, W. Wen, T. White, I. Agartz, O. A. Andreassen, J. Blangero, D. I. Boomsma, R. M. Brouwer, D. M. Cannon, M. R. Cookson, E. J. C. de Geus, I. J. Deary, G. Donohoe, G. Fernández, S. E. Fisher, C. Francks, D. C. Glahn, H. J. Grabe, O. Gruber, J. Hardy, R. Hashimoto, H. E. Hulshoff Pol, E. G. Jönsson, I. Kloszewska, S. Lovestone, V. S. Mattay, P. Mecocci, C. McDonald, A. M. McIntosh, R. A. Ophoff, T. Paus, Z. Pausova, M. Ryten, P. S. Sachdev, A. J. Saykin, A. Simmons, A. Singleton, H. Soininen, J. M. Wardlaw, M. E. Weale, D. R. Weinberger, H. H. H. Adams, L. J. Launer, S. Seiler, R. Schmidt, G. Chauhan, C. L. Satizabal, J. T. Becker, L. Yanek, S. J. van der Lee, M. Ebling, B. Fischl, W. T. Longstreth, D. Greve, H. Schmidt, P. Nyquist, L. N. Vinke, C. M. van Duijn, L. Xue, B. Mazoyer, J. C. Bis, V. Gudnason, S. Seshadri, M. A. Ikram; Alzheimer's Disease Neuroimaging Initiative; CHARGE Consortium; EPIGEN; IMAGEN; SYS; N. G. Martin, M. J. Wright, G. Schumann, B. Franke, P. M. Thompson, S. E. Medland, Common genetic variants influence human subcortical brain structures. *Nature* **520**, 224–229 (2015).

4. C. L. Satizabal, H. H. H. Adams, D. P. Hibar, C. C. White, M. J. Knol, J. L. Stein, M. Scholz, M. Sargurupremraj, N. Jahanshad, G. V. Roshchupkin, A. V. Smith, J. C. Bis, X. Jian, M. Luciano, E. Hofer, A. Teumer, S. J. Van Der Lee, J. Yang, L. R. Yanek, T. V. Lee, S. Li, Y. Hu, J. Y. Koh, J. D. Eicher, S. Desrivières, A. Arias-Vasquez, G. Chauhan, L. Athanasiu, M. E. Rentería, S. Kim, D. Hoehn, N. J. Armstrong, Q. Chen, A. J. Holmes, A. Den Braber, I. Kloszewska, M. Andersson, T. Espeseth, O. Grimm, L. Abramovic, S. Alhusaini, Y. Milaneschi, M. Papmeyer, T. Axelsson, S. Ehrlich, R. Roiz-Santiañez, B. Kraemer, A. K. Håberg, H. J. Jones, G. B. Pike, D. J. Stein, A. Stevens, J. Bralten, M. W. Vernooij, T. B. Harris, I. Filippi, A. V. Witte, T. Guadalupe, K. Wittfeld, T. H. Mosley, J. T. Becker, N. T. Doan, S. P. Hagenaars, Y. Saba, G. Cuellar-Partida, N. Amin, S. Hilal, K. Nho, N. Mirza-Schreiber, K. Arfanakis, D. M. Becker, D. Ames, A. L. Goldman, P. H. Lee, D. I. Boomsma, S. Lovestone, S. Giddaluru, S. Le Hellard, M. Mattheisen, M. M. Bohlken, D. Kasperaviciute, L. Schmaal, S. M. Lawrie, I. Agartz, E. Walton, D. Tordesillas-Gutierrez, G. E. Davies, J. Shin, J. C. Ipser, L. N. Vinke, M. Hoogman, T. Jia, R. Burkhardt, M. Klein, F. Crivello, D. Janowitz, O. Carmichael, U. K. Haukvik, B. S. Aribisala, H. Schmidt, L. T. Strike, C.-Y. Cheng, S. L. Risacher, B. Pütz, D. A. Fleischman, A. A. Assareh, V. S. Mattay, R. L. Buckner, P. Mecocci, A. M. Dale, S. Cichon, M. P. Boks, M. Matarin, B. W. J. H. Penninx, V. D. Calhoun, M. M. Chakravarty, A. F. Marquand, C. Macare, S. K. Masouleh, J. Oosterlaan, P. Amouyel, K. Hegenscheid, J. I. Rotter, A. J. Schork, D. C. M. Liewald, G. I. De Zubicaray, T. Y. Wong, L. Shen, P. G. Sämann, H. Brodaty, J. L. Roffman, E. J. C. De Geus, M. Tsolaki, S. Erk, K. R. Van Eijk, G. L. Cavalleri, N. J. A. Van Der Wee, A. M. McIntosh, R. L. Gollub, K. B. Bulayeva, M. Bernard, J. S. Richards, J. J. Himali, M. Loeffler, N. Rommelse, W. Hoffmann, L. T. Westlye, M. C. Valdés Hernández, N. K. Hansell, T. G. M. Van Erp, C. Wolf, J. B. J. Kwok, B. Vellas, A. Heinz, L. M. Olde Loohuis, N. Delanty, B.-C. Ho, C. R. K. Ching, E. Shumskaya, B. Singh, A. Hofman, D. Van Der Meer, G. Homuth, B. M. Psaty, M. E. Bastin, G. W. Montgomery, T. M. Foroud, S. Reppermund, J.-J. Hottenga, A. Simmons, A. Meyer-Lindenberg, W. Cahn, C. D. Whelan, M. M. J. Van Donkelaar, Q. Yang, N. Hosten, R. C. Green, A. Thalamuthu, S. Mohnke, H. E. Hulshoff Pol, H. Lin, C. R. Jack, P. R. Schofield, T. W. Mühleisen, P. Maillard, S. G. Potkin, W. Wen, E. Fletcher, A. W. Toga, O. Gruber, M. Huentelman, G. Davey Smith, L. J. Launer, L. Nyberg, E. G. Jönsson, B. Crespo-Facorro, N. Koen, D. N. Greve, A. G. Uitterlinden, D. R. Weinberger, V. M. Steen, I. O. Fedko, N. A. Groenewold, W. J. Niessen, R. Toro, C. Tzourio, W. T. Longstreth, M. K. Ikram, J. W. Smoller, M.-J. Van Tol, J. E. Sussmann, T. Paus, H. Lemaître, M. L. Schroeter, B. Mazoyer, O. A. Andreassen, F. Holsboer, C. Depondt, D. J. Veltman, J. A. Turner, Z. Pausova, G. Schumann, D. Van Rooij, S. Djurovic, I. J. Deary, K. L. McMahon, B. Müller-Myhsok, R. M. Brouwer, H. Soininen, M. Pandolfo, T. H. Wassink, J. W. Cheung, T. Wolfers, J.-L. Martinot, M. P. Zwiers, M. Nauck, I. Melle, N. G. Martin, R. Kanai, E. Westman, R. S. Kahn, S. M. Sisodiya, T. White, A. Saremi, H. Van Bokhoven, H. G. Brunner, H. Völzke, M. J. Wright, D. Van'T Ent, M. M. Nöthen, R. A. Ophoff, J. K. Buitelaar, G. Fernández, P. S. Sachdev, M. Rietschel, N. E. M. Van Haren, S. E. Fisher, A. S. Beiser, C. Francks, A. J. Saykin, K. A. Mather, N. Romanczuk-Seiferth, C. A. Hartman, A. L. DeStefano, D. J. Heslenfeld, M. W. Weiner, H. Walter, P. J. Hoekstra, P. A. Nyquist, B. Franke, D. A. Bennett, H. J. Grabe, A. D. Johnson, C. Chen, C. M. Van Duijn, O. L. Lopez, M. Fornage, J. M. Wardlaw, R. Schmidt, C. DeCarli, P. L. De Jager, A. Villringer, S. Debette, V. Gudnason, S. E. Medland, J. M. Shulman, P. M. Thompson, S. Seshadri, M. A. Ikram, Genetic architecture of subcortical brain structures in 38,851 individuals. *Nat. Genet.* **51**, 1624–1636 (2019).
5. T. Elvsåshagen, S. Bahrami, D. Van Der Meer, I. Agartz, D. Alnæs, D. M. Barch, R. Baur-Streubel, A. Bertolino, M. K. Beyer, G. Blasi, S. Borgwardt, B. Boye, J. Buitelaar, E. Bøen, E. G. Celius, S. Cervenka, A. Conzelmann, D. Coynel, P. Di Carlo, S. Djurovic, S. Eisenacher, T. Espeseth, H. Fatouros-Bergman, L. Flyckt, B. Franke, O. Frei, B. Gelao, H. F. Harbo, C. A. Hartman, A. Håberg, D. Heslenfeld, P. J. Hoekstra, E. A. Høgestøl, R. Jonassen, E. G. Jönsson, Karolinska Schizophrenia Project (KaSP) consortium, L. Farde, L. Flyckt, G. Engberg, H. Fatouros-Bergman, S. Cervenka, L. Schwieler, F. Piehl, I. Agartz, K. Collste, P. Victorsson, A. Malmqvist, M. Hedberg, F. Orhan, C. M. Sellgren, P. Kirsch, I. Kłoszewska, T. V. Lagerberg, N. I. Landrø, S. Le Hellard, K.-P. Lesch, L. A. Maglanoc, U. F. Malt, P. Mecocci, I. Melle, A. Meyer-Lindenberg, T. Moberget, J. E. Nordvik, L. Nyberg, K. S. O. Connell, J. Oosterlaan, M. Papalino, A. Papassotiropoulos, P. Pauli, G. Pergola, K. Persson, D. De Quervain, A. Reif, J. Rokicki, D. Van Rooij, A. A. Shadrin, A. Schmidt, E. Schwarz, G. Selbæk, H. Soininen, P. Sowa, V. M. Steen, M. Tsolaki, B. Vellas, L. Wang, E. Westman, G. C. Ziegler, M. Zink, O. A. Andreassen, L. T. Westlye, T. Kaufmann, The genetic architecture of human brainstem structures and their involvement in common brain disorders. *Nat. Commun.* **11**, 4016 (2020).
6. T. Ge, M. Reuter, A. M. Winkler, A. J. Holmes, P. H. Lee, L. S. Tirrell, J. L. Roffman, R. L. Buckner, J. W. Smoller, M. R. Sabuncu, Multidimensional heritability analysis of neuroanatomical shape. *Nat. Commun.* **7**, 13291 (2016).
7. G. V. Roshchupkin, B. A. Gutman, M. W. Vernooij, N. Jahanshad, N. G. Martin, A. Hofman, K. L. McMahon, S. J. Van Der Lee, C. M. Van Duijn, G. I. De Zubicaray, A. G. Uitterlinden, M. J. Wright, W. J. Niessen, P. M. Thompson, M. A. Ikram, H. H. H. Adams, Heritability of the shape of subcortical brain structures in the general population. *Nat. Commun.* **7**, 13738 (2016).
8. B. A. Gutman, T. G. M. Van Erp, K. Alpert, C. R. K. Ching, D. Isaev, A. Ragothaman, N. Jahanshad, A. Saremi, A. Zavaliangos-Petropulu, D. C. Glahn, L. Shen, S. Cong, D. Alnæs, O. A. Andreassen, N. T. Doan, L. T. Westlye, P. Kochunov, T. D. Satterthwaite, D. H. Wolf, A. J. Huang, C. Kessler, A. Weideman, D. Nguyen, B. A. Mueller, L. Faziola, S. G. Potkin, A. Preda, D. H. Mathalon, J. Bustillo, V. Calhoun, J. M. Ford, E. Walton, S. Ehrlich, G. Ducci, N. Banaj, F. Piras, F. Piras, G. Spalletta, E. J. Canales-Rodríguez, P. Fuentes-Claramonte, E. Pomarol-Clotet, J. Radua, R. Salvador, S. Sarró, E. W. Dickie, A. Voineskos, D. Tordesillas-Gutiérrez, B. Crespo-Facorro, E. Setién-Suero, J. M. Van Son, S. Borgwardt, F. Schönborn-Harrisberger, D. Morris, G. Donohoe, L. Holleran, D. Cannon, C. McDonald, A. Corvin, M. Gill, G. B. Filho, P. G. P. Rosa, M. H. Serpa, M. V. Zanetti, I. Lebedeva, V. Kaleda, A. Tomyshev, T. Crow, A. James, S. Cervenka, C. M. Sellgren, H. Fatouros-Bergman, I. Agartz, F. Howells, D. J. Stein, H. Temmingh, A. Uhlmann, G. I. De Zubicaray, K. L. McMahon, M. Wright, D. Cobia, J. G. Csernansky, P. M. Thompson, J. A. Turner, L. Wang, A meta-analysis of deep brain structural shape and asymmetry abnormalities in 2,833 individuals with schizophrenia compared with 3,929 healthy volunteers via the ENIGMA Consortium. *Hum. Brain Mapp.* **43**, 352–372 (2022).
9. L. T. Elliott, K. Sharp, F. Alfaro-Almagro, S. Shi, K. L. Miller, G. Douaud, J. Marchini, S. M. Smith, Genome-wide association studies of brain imaging phenotypes in UK Biobank. *Nature* **562**, 210–216 (2018).
10. C. C. Fan, R. Loughnan, C. Makowski, D. Pecheva, C.-H. Chen, D. J. Hagler Jr., W. K. Thompson, N. Parker, D. van der Meer, O. Frei, O. A. Andreassen, A. M. Dale, Multivariate genome-wide association study on tissue-sensitive diffusion metrics highlights pathways that shape the human brain. *Nat. Commun.* **13**, 2423 (2022).
11. S. Goovaerts, H. Hoskens, R. J. Eller, N. Herrick, A. M. Musolf, C. M. Justice, M. Yuan, S. Naqvi, M. K. Lee, D. Vandermeulen, H. L. Szabo-Rogers, P. A. Romitti, S. A. Boyadjiev, M. L. Marazita, J. R. Shaffer, M. D. Shriver, J. Wysocka, S. Walsh, S. M. Weinberg, P. Claes, Joint multi-ancestry and admixed GWAS reveals the complex genetics behind human cranial vault shape. *Nat. Commun.* **14**, 7436 (2023).
12. S. Naqvi, Y. Sleyp, H. Hoskens, K. Indencleef, J. P. Spence, R. Bruffaerts, A. Radwan, R. J. Eller, S. Richmond, M. D. Shriver, J. R. Shaffer, S. M. Weinberg, S. Walsh, J. Thompson, J. K. Pritchard, S. Sunaert, H. Peeters, J. Wysocka, P. Claes, Shared heritability of human face and brain shape. *Nat. Genet.* **53**, 830–839 (2021).
13. M. Reuter, F.-E. Wolter, N. Peinecke, Laplace–Beltrami spectra as 'Shape-DNA' of surfaces and solids. *Computer-Aided Design* **38**, 342–366 (2006).
14. M. Reuter, F.-E. Wolter, N. Peinecke, "Laplace-spectra as fingerprints for shape matching," in *Proceedings of the 2005 ACM Symposium on Solid and Physical Modeling* (ACM, 2005), pp. 101–106.
15. M. Reuter, F.-E. Wolter, M. Shenton, M. Niethammer, Laplace–Beltrami eigenvalues and topological features of eigenfunctions for statistical shape analysis. *Comput.-Aided Des.* **41**, 739–755 (2009).
16. E. F. F. Chladni, *Entdeckungen über die Theorie des Klanges* (bey Weidmanns Erben und Reich, 1787).
17. M. Kac, Can one hear the shape of a drum? *Am. Math. Monthly* **73**, 1–23 (1966).
18. C. Gordon, D. L. Webb, S. Wolpert, One cannot hear the shape of a drum. *Bull. Amer. Math. Soc.* **27**, 134–138 (1992).
19. S. Zelditch, Inverse spectral problem for analytic domains, II: $\mathbb{Z}_2$-symmetric domains. *Ann. Math.* **170**, 205–269 (2009).
20. H. P. McKean Jr., I. M. Singer, Curvature and the eigenvalues of the Laplacian. *J. Differential Geom.* **1**, 43–69 (1967).
21. C. Wachinger, P. Golland, W. Kremen, B. Fischl, M. Reuter, Alzheimer's Disease Neuroimaging Initiative, BrainPrint: A discriminative characterization of brain morphology. *Neuroimage* **109**, 232–248 (2015).
22. J. C. Pang, K. M. Aquino, M. Oldehinkel, P. A. Robinson, B. D. Fulcher, M. Breakspear, A. Fornito, Geometric constraints on human brain function. *Nature* **618**, 566–574 (2023).
23. D. Van Der Meer, A. A. Shadrin, K. O'Connell, F. Bettella, S. Djurovic, T. Wolfers, D. Alnæs, I. Agartz, O. B. Smeland, I. Melle, J. M. Sánchez, D. E. J. Linden, A. M. Dale, L. T. Westlye, O. A. Andreassen, O. Frei, T. Kaufmann, Boosting schizophrenia genetics by utilizing genetic overlap with brain morphology. *Biol. Psychiatry* **92**, 291–298 (2022).
24. S. Bahrami, K. Nordengen, A. A. Shadrin, O. Frei, D. Van Der Meer, A. M. Dale, L. T. Westlye, O. A. Andreassen, T. Kaufmann, Distributed genetic architecture across the hippocampal formation implies common neuropathology across brain disorders. *Nat. Commun.* **13**, 3436 (2022).
25. T. Elvsåshagen, A. Shadrin, O. Frei, D. Van Der Meer, S. Bahrami, V. J. Kumar, O. Smeland, L. T. Westlye, O. A. Andreassen, T. Kaufmann, The genetic architecture of the human thalamus and its overlap with ten common brain disorders. *Nat. Commun.* **12**, 2909 (2021).
26. H. H. Yin, B. J. Knowlton, The role of the basal ganglia in habit formation. *Nat. Rev. Neurosci.* **7**, 464–476 (2006).
27. L. T. Grinberg, U. Rueb, H. Heinsen, Brainstem: Neglected locus in neurodegenerative diseases. *Front. Neurol.* **2**, 42 (2011).
28. K. Watanabe, E. Taskesen, A. van Bochoven, D. Posthuma, Functional mapping and annotation of genetic associations with FUMA. *Nat. Commun.* **8**, 1826 (2017).
29. K. Wang, M. Li, H. Hakonarson, ANNOVAR: Functional annotation of genetic variants from high-throughput sequencing data. *Nucleic Acids Res.* **38**, e164 (2010).

30. M. Kircher, D. M. Witten, P. Jain, B. J. O'Roak, G. M. Cooper, J. Shendure, A general framework for estimating the relative pathogenicity of human genetic variants. *Nat. Genet.* **46**, 310–315 (2014).
31. M. J. Landrum, S. Chitipiralla, G. R. Brown, C. Chen, B. Gu, J. Hart, D. Hoffman, W. Jang, K. Kaur, C. Liu, V. Lyoshin, Z. Maddipatla, R. Maiti, J. Mitchell, N. O'Leary, G. R. Riley, W. Shi, G. Zhou, V. Schneider, D. Maglott, J. B. Holmes, B. L. Kattman, ClinVar: Improvements to accessing data. *Nucleic Acids Res.* **48**, D835–D844 (2020).
32. J. Cheng, G. Novati, J. Pan, C. Bycroft, A. Žemgulytė, T. Applebaum, A. Pritzel, L. H. Wong, M. Zielinski, T. Sargeant, R. G. Schneider, A. W. Senior, J. Jumper, D. Hassabis, P. Kohli, Ž. Avsec, Accurate proteome-wide missense variant effect prediction with AlphaMissense. *Science* **381**, eadg7492 (2023).
33. Schizophrenia Working Group of the Psychiatric Genomics Consortium, Biological insights from 108 schizophrenia-associated genetic loci. *Nature* **511**, 421–427 (2014).
34. N. Carrera, M. Arrojo, J. Sanjuán, R. Ramos-Ríos, E. Paz, J. J. Suárez-Rama, M. Páramo, S. Agra, J. Brenlla, S. Martínez, O. Rivero, D. A. Collier, A. Palotie, S. Cichon, M. M. Nöthen, M. Rietschel, D. Rujescu, H. Stefansson, S. Steinberg, E. Sigurdsson, D. St. Clair, S. Tosato, T. Werge, K. Stefansson, J. C. González, J. Valero, A. Gutiérrez-Zotes, A. Labad, L. Martorell, E. Vilella, Á. Carracedo, J. Costas, Association study of nonsynonymous single nucleotide polymorphisms in schizophrenia. *Biol. Psychiatry* **71**, 169–177 (2012).
35. A. F. Pardiñas, P. Holmans, A. J. Pocklington, V. Escott-Price, S. Ripke, N. Carrera, S. E. Legge, S. Bishop, D. Cameron, M. L. Hamshere, J. Han, L. Hubbard, A. Lynham, K. Mantripragada, E. Rees, J. H. M. Cabe, S. A. Mc Carroll, B. T. Baune, G. Breen, E. M. Byrne, U. Dannlowski, T. C. Eley, C. Hayward, N. G. Martin, A. M. Mc Intosh, R. Plomin, D. J. Porteous, N. R. Wray, A. Caballero, D. H. Geschwind, L. M. Huckins, D. M. Ruderfer, E. Santiago, P. Sklar, E. A. Stahl, H. Won, E. Agerbo, T. D. Als, O. A. Andreassen, M. Bækvad-Hansen, P. B. Mortensen, C. B. Pedersen, A. D. Børglum, J. Bybjerg-Grauholm, S. Djurovic, N. Durmishi, M. G. Pedersen, V. Golimbet, J. Grove, D. M. Hougaard, M. Mattheisen, E. Molden, O. Mors, M. Nordentoft, M. Pejovic-Milovancevic, E. Sigurdsson, T. Silagadze, C. S. Hansen, K. Stefansson, H. Stefansson, S. Steinberg, S. Tosato, T. Werge, GERAD Consortium, CRESTAR Consortium, D. A. Collier, D. Rujescu, G. Kirov, M. J. Owen, M. C. O'Donovan, J. T. R. Walters, Common schizophrenia alleles are enriched in mutation-intolerant genes and in regions under strong background selection. *Nat. Genet.* **50**, 381–389 (2018).
36. D. Li, J.-P. Achkar, T. Haritunians, J. P. Jacobs, K. Y. Hui, M. D'Amato, S. Brand, G. Radford-Smith, J. Halfvarson, J.-H. Niess, S. Kugathasan, C. Büning, L. P. Schumm, L. Klei, A. Ananthakrishnan, G. Aumais, L. Baidoo, M. Dubinsky, C. Fiocchi, J. Glas, R. Milgrom, D. D. Proctor, M. Regueiro, L. A. Simms, J. M. Stempak, S. R. Targan, L. Törkvist, Y. Sharma, B. Devlin, J. Borneman, H. Hakonarson, R. J. Xavier, M. Daly, S. R. Brant, J. D. Rioux, M. S. Silverberg, J. H. Cho, J. Braun, D. P. McGovern, R. H. Duerr, A pleiotropic missense variant in SLC39A8 is associated with Crohn's disease and human gut microbiome composition. *Gastroenterology* **151**, 724–732 (2016).
37. The International Consortium for Blood Pressure Genome-Wide Association Studies, Genetic variants in novel pathways influence blood pressure and cardiovascular disease risk. *Nature* **478**, 103–109 (2011).
38. T. M. Caffrey, R. Wade-Martins, Functional MAPT haplotypes: Bridging the gap between genotype and neuropathology. *Neurobiol. Dis.* **27**, 1–10 (2007).
39. S.-H. Lin, D. W. Brown, M. J. Machiela, LDtrait: An online tool for identifying published phenotype associations in linkage disequilibrium. *Cancer Res.* **80**, 3443–3446 (2020).
40. M. Wainberg, N. J. Forde, S. Mansour, I. Kerrebijn, S. E. Medland, C. Hawco, S. J. Tripathy, Genetic architecture of the structural connectome. *Nat. Commun.* **15**, 1962 (2024).
41. C. A. de Leeuw, J. M. Mooij, T. Heskes, D. Posthuma, MAGMA: Generalized gene-set analysis of GWAS data. *PLOS Comput. Biol.* **11**, e1004219 (2015).
42. T. Rittman, M. Rubinov, P. E. Vértes, A. X. Patel, C. E. Ginestet, B. C. P. Ghosh, R. A. Barker, M. G. Spillantini, E. T. Bullmore, J. B. Rowe, Regional expression of the MAPT gene is associated with loss of hubs in brain networks and cognitive impairment in Parkinson disease and progressive supranuclear palsy. *Neurobiol. Aging* **48**, 153–160 (2016).
43. R. S. Desikan, A. J. Schork, Y. Wang, A. Witoelar, M. Sharma, L. K. McEvoy, D. Holland, J. B. Brewer, C.-H. Chen, W. K. Thompson, D. Harold, J. Williams, M. J. Owen, M. C. O'Donovan, M. A. Pericak-Vance, R. Mayeux, J. L. Haines, L. A. Farrer, G. D. Schellenberg, P. Heutink, A. B. Singleton, A. Brice, N. W. Wood, J. Hardy, M. Martinez, S. H. Choi, A. DeStefano, M. A. Ikram, J. C. Bis, A. Smith, A. L. Fitzpatrick, L. Launer, C. Van Duijn, S. Seshadri, I. D. Ulstein, D. Aarsland, T. Fladby, S. Djurovic, B. T. Hyman, J. Snaedal, H. Stefansson, K. Stefansson, T. Gasser, O. A. Andreassen, A. M. Dale, ADNI ADGC, GERAD, CHARGE and IPDGC Investigators, Genetic overlap between Alzheimer's disease and Parkinson's disease at the MAPT locus. *Mol. Psychiatry* **20**, 1588–1595 (2015).
44. E. M. Weeks, J. C. Ulirsch, N. Y. Cheng, B. L. Trippe, R. S. Fine, J. Miao, T. A. Patwardhan, M. Kanai, J. Nasser, C. P. Fulco, K. C. Tashman, F. Aguet, T. Li, J. Ordovas-Montanes, C. S. Smillie, M. Biton, A. K. Shalek, A. N. Ananthakrishnan, R. J. Xavier, A. Regev, R. M. Gupta, K. Lage, K. G. Ardlie, J. N. Hirschhorn, E. S. Lander, J. M. Engreitz, H. K. Finucane, Leveraging polygenic enrichments of gene features to predict genes underlying complex traits and diseases. *Nat. Genet.* **55**, 1267–1276 (2023).
45. Z. Sha, D. Schijven, S. E. Fisher, C. Francks, Genetic architecture of the white matter connectome of the human brain. *Sci. Adv.* **9**, eadd2870 (2023).
46. Y. Benjamini, Y. Hochberg, Controlling the false discovery rate: A practical and powerful approach to multiple testing. *J. R. Stat. Soc. B. Methodol.* **57**, 289–300 (1995).
47. Y. Wu, K. S. Burch, A. Ganna, P. Pajukanta, B. Pasaniuc, S. Sankararaman, Fast estimation of genetic correlation for biobank-scale data. *Am. J. Human Genet.* **109**, 24–32 (2022).
48. C. Palmer, I. Pe'er, Statistical correction of the Winner's Curse explains replication variability in quantitative trait genome-wide association studies. *PLOS Genet.* **13**, e1006916 (2017).
49. D. van der Meer, J. Rokicki, T. Kaufmann, A. Córdova-Palomera, T. Moberget, D. Alnæs, F. Bettella, O. Frei, N. T. Doan, I. E. Sønderby, O. B. Smeland, I. Agartz, A. Bertolino, J. Bralten, C. L. Brandt, J. K. Buitelaar, S. Djurovic, M. van Donkelaar, E. S. Dørum, T. Espeseth, S. V. Faraone, G. Fernández, S. E. Fisher, B. Franke, B. Haatveit, C. A. Hartman, P. J. Hoekstra, A. K. Håberg, E. G. Jönsson, K. K. Kolskår, S. Le Hellard, M. J. Lund, A. J. Lundervold, A. Lundervold, I. Melle, J. Monereo Sánchez, L. C. Norbom, J. E. Nordvik, L. Nyberg, J. Oosterlaan, M. Papalino, A. Papassotiropoulos, G. Pergola, D. J. F. de Quervain, G. Richard, A.-M. Sanders, P. Selvaggi, E. Shumskaya, V. M. Steen, S. Tønnesen, K. M. Ulrichsen, M. P. Zwiers, O. A. Andreassen, L. T. Westlye; Alzheimer's Disease Neuroimaging Initiative; Pediatric Imaging, Neurocognition and Genetics Study, Brain scans from 21,297 individuals reveal the genetic architecture of hippocampal subfield volumes. *Mol. Psychiatry* **25**, 3053–3065 (2020).
50. M. Lanfranchi, S. Yandiev, G. Meyer-Dilhet, S. Ellouze, M. Kerkhofs, R. Dos Reis, A. Garcia, C. Blondet, A. Amar, A. Kneppers, H. Polvèche, D. Plassard, M. Foretz, B. Viollet, K. Sakamoto, R. Mounier, C. F. Bourgeois, O. Raineteau, E. Goillot, J. Courchet, The AMPK-related kinase NUAK1 controls cortical axons branching by locally modulating mitochondrial metabolic functions. *Nat. Commun.* **15**, 2487 (2024).
51. C. Makowski, H. Wang, A. Srinivasan, A. Qi, Y. Qiu, D. van der Meer, O. Frei, J. Zou, P. M. Visscher, J. Yang, C.-H. Chen, Larger cerebral cortex is genetically correlated with greater frontal area and dorsal thickness. *Proc. Natl. Acad. Sci. U.S.A.* **120**, e2214834120 (2023).
52. A. Okbay, Y. Wu, N. Wang, H. Jayashankar, M. Bennett, S. M. Nehzati, J. Sidorenko, H. Kweon, G. Goldman, T. Gjorgjieva, Y. Jiang, B. Hicks, C. Tian, D. A. Hinds, R. Ahlskog, P. K. E. Magnusson, S. Oskarsson, C. Hayward, A. Campbell, D. J. Porteous, J. Freese, P. Herd, C. Watson, J. Jala, D. Conley, P. D. Koellinger, M. Johannesson, D. Laibson, M. N. Meyer, J. J. Lee, A. Kong, L. Yengo, D. Cesarini, P. Turley, P. M. Visscher, J. P. Beauchamp, D. J. Benjamin, A. I. Young, Polygenic prediction of educational attainment within and between families from genome-wide association analyses in 3 million individuals. *Nat. Genet.* **54**, 437–449 (2022).
53. M. P. M. Soutar, D. Melandri, B. O'Callaghan, E. Annuario, A. E. Monaghan, N. J. Welsh, K. D'Sa, S. Guelfi, D. Zhang, A. Pittman, D. Trabzuni, A. H. A. Verboven, K. S. Pan, D. A. Kia, M. Bictash, S. Gandhi, H. Houlden, M. R. Cookson, N. N. Kasri, N. W. Wood, A. B. Singleton, J. Hardy, P. J. Whiting, C. Blauwendraat, A. J. Whitworth, C. Manzoni, M. Ryten, P. A. Lewis, H. Plun-Favreau, Regulation of mitophagy by the NSL complex underlies genetic risk for Parkinson's disease at 16q11.2 and MAPT H1 loci. *Brain* **145**, 4349–4367 (2022).
54. M. Baker, I. Litvan, H. Houlden, J. Adamson, D. Dickson, J. Perez-Tur, J. Hardy, T. Lynch, E. Bigio, M. Hutton, Association of an extended haplotype in the tau gene with progressive supranuclear palsy. *Hum. Mol. Genet.* **8**, 711–715 (1999).
55. A. M. Pittman, A. J. Myers, J. Duckworth, L. Bryden, M. Hanson, P. Abou-Sleiman, N. W. Wood, J. Hardy, A. Lees, R. de Silva, The structure of the tau haplotype in controls and in progressive supranuclear palsy. *Hum. Mol. Genet.* **13**, 1267–1274 (2004).
56. A. M. Pittman, A. J. Myers, P. Abou-Sleiman, H. C. Fung, M. Kaleem, L. Marlowe, J. Duckworth, D. Leung, D. Williams, L. Kilford, N. Thomas, C. M. Morris, D. Dickson, N. W. Wood, J. Hardy, A. J. Lees, R. de Silva, Linkage disequilibrium fine mapping and haplotype association analysis of the tau gene in progressive supranuclear palsy and corticobasal degeneration. *J. Med. Genet.* **42**, 837–846 (2005).
57. P. Pastor, M. Ezquerra, J. C. Perez, S. Chakraverty, J. Norton, B. A. Racette, D. McKeel, J. S. Perlmutter, E. Tolosa, A. M. Goate, Novel haplotypes in 17q21 are associated with progressive supranuclear palsy. *Ann. Neurol.* **56**, 249–258 (2004).
58. M. G. Spillantini, J. R. Murrell, M. Goedert, M. R. Farlow, A. Klug, B. Ghetti, Mutation in the tau gene in familial multiple system tauopathy with presenile dementia. *Proc. Natl. Acad. Sci. U.S.A.* **95**, 7737–7741 (1998).
59. J. Simón-Sánchez, C. Schulte, J. M. Bras, M. Sharma, J. R. Gibbs, D. Berg, C. Paisan-Ruiz, P. Lichtner, S. W. Scholz, D. G. Hernandez, R. Krüger, M. Federoff, C. Klein, A. Goate, J. Perlmutter, M. Bonin, M. A. Nalls, T. Illig, C. Gieger, H. Houlden, M. Steffens, M. S. Okun, B. A. Racette, M. R. Cookson, K. D. Foote, H. H. Fernandez, B. J. Traynor, S. Schreiber, S. Arepalli, R. Zonozi, K. Gwinn, M. van der Brug, G. Lopez, S. J. Chanock, A. Schatzkin, Y. Park, A. Hollenbeck, J. Gao, X. Huang, N. W. Wood, D. Lorenz, G. Deuschl, H. Chen, O. Riess, J. A. Hardy, A. B. Singleton, T. Gasser, Genome-wide association study reveals genetic risk underlying Parkinson's disease. *Nat. Genet.* **41**, 1308–1312 (2009).
60. P. Sánchez-Juan, S. Moreno, I. de Rojas, I. Hernández, S. Valero, M. Alegret, L. Montrreal, P. García González, C. Lage, S. López-García, E. Rodrííguez-Rodríguez, A. Orellana, L. Tárraga, M. Boada, A. Ruiz, The MAPT H1 haplotype is a risk factor for Alzheimer's disease in APOE ε4 non-carriers. *Front. Aging Neurosci.* **11**, 327 (2019).

61. N. Kouri, O. A. Ross, B. Dombroski, C. S. Younkin, D. J. Serie, A. Soto-Ortolaza, M. Baker, N. C. A. Finch, H. Yoon, J. Kim, S. Fujioka, C. A. McLean, B. Ghetti, S. Spina, L. B. Cantwell, M. R. Farlow, J. Grafman, E. D. Huey, M. Ryung Han, S. Beecher, E. T. Geller, H. A. Kretzschmar, S. Roeber, M. Gearing, J. L. Juncos, J. P. G. Vonsattel, V. M. Van Deerlin, M. Grossman, H. I. Hurtig, R. G. Gross, S. E. Arnold, J. Q. Trojanowski, V. M. Lee, G. K. Wenning, C. L. White, G. U. Höglinger, U. Müller, B. Devlin, L. I. Golbe, J. Crook, J. E. Parisi, B. F. Boeve, K. A. Josephs, Z. K. Wszolek, R. J. Uitti, N. R. Graff-Radford, I. Litvan, S. G. Younkin, L.-S. Wang, N. Ertekin-Taner, R. Rademakers, H. Hakonarsen, G. D. Schellenberg, D. W. Dickson, Genome-wide association study of corticobasal degeneration identifies risk variants shared with progressive supranuclear palsy. *Nat. Commun.* **6**, 7247 (2015).
62. C. Bellenguez, F. Küçükali, I. E. Jansen, L. Kleineidam, S. Moreno-Grau, N. Amin, A. C. Naj, R. Campos-Martin, B. Grenier-Boley, V. Andrade, P. A. Holmans, A. Boland, V. Damotte, S. J. van der Lee, M. R. Costa, T. Kuulasmaa, Q. Yang, I. de Rojas, J. C. Bis, A. Yaqub, I. Prokic, J. Chapuis, S. Ahmad, V. Giedraitis, D. Aarsland, P. Garcia-Gonzalez, C. Abdelnour, E. Alarcón-Martín, D. Alcolea, M. Alegret, I. Alvarez, V. Álvarez, N. J. Armstrong, A. Tsolaki, C. Antúnez, I. Appollonio, M. Arcaro, S. Archetti, A. A. Pastor, B. Arosio, L. Athanasiu, H. Bailly, N. Banaj, M. Baquero, S. Barral, A. Beiser, A. B. Pastor, J. E. Below, P. Benchek, L. Benussi, C. Berr, C. Besse, V. Bessi, G. Binetti, A. Bizarro, R. Blesa, M. Boada, E. Boerwinkle, B. Borroni, S. Boschi, P. Bossù, G. Bråthen, J. Bressler, C. Bresner, H. Brodaty, K. J. Brookes, L. I. Brusco, D. Buiza-Rueda, K. Bûrger, V. Burholt, W. S. Bush, M. Calero, L. B. Cantwell, G. Chene, J. Chung, M. L. Cuccaro, Á. Carracedo, R. Cecchetti, L. Cervera-Carles, C. Charbonnier, H.-H. Chen, C. Chillotti, S. Ciccone, J. A. H. R. Claassen, C. Clark, E. Conti, A. Corma-Gómez, E. Costantini, C. Custodero, D. Daian, M. C. Dalmasso, A. Daniele, E. Dardiotis, J.-F. Dartigues, P. P. de Deyn, K. de Paiva Lopes, L. D. de Witte, S. Debette, J. Deckert, T. del Ser, N. Denning, A. DeStefano, M. Dichgans, J. Diehl-Schmid, M. Diez-Fairen, P. D. Rossi, S. Djurovic, E. Duron, E. Düzel, C. Dufouil, G. Eiriksdottir, S. Engelborghs, V. Escott-Price, A. Espinosa, M. Ewers, K. M. Faber, T. Fabrizio, S. F. Nielsen, D. W. Fardo, L. Farotti, C. Fenoglio, M. Fernández-Fuertes, R. Ferrari, C. B. Ferreira, E. Ferri, B. Fin, P. Fischer, T. Fladby, K. Fließbach, B. Fongang, M. Fornage, J. Fortea, T. M. Foroud, S. Fostinelli, N. C. Fox, E. Franco-Macías, M. J. Bullido, A. Frank-García, L. Froelich, B. Fulton-Howard, D. Galimberti, J. M. García-Alberca, P. García-González, S. Garcia-Madrona, G. Garcia-Ribas, R. Ghidoni, I. Giegling, G. Giorgio, A. M. Goate, O. Goldhardt, D. Gomez-Fonseca, A. González-Pérez, C. Graff, G. Grande, E. Green, T. Grimmer, E. Grünblatt, M. Grunin, V. Gudnason, T. Guetta-Baranes, A. Haapasalo, G. Hadjigeorgiou, J. L. Haines, K. L. Hamilton-Nelson, H. Hampel, O. Hanon, J. Hardy, A. M. Hartmann, L. Hausner, J. Harwood, S. Heilmann-Heimbach, S. Helisalmi, M. T. Heneka, I. Hernández, M. J. Herrmann, P. Hoffmann, C. Holmes, H. Holstege, R. H. Vilas, M. Hulsman, J. Humphrey, G. J. Biessels, X. Jian, C. Johansson, G. R. Jun, Y. Kastumata, J. Kauwe, P. G. Kehoe, L. Kilander, A. K. Ståhlbom, M. Kivipelto, A. Koivisto, J. Kornhuber, M. H. Kosmidis, W. A. Kukull, P. P. Kuksa, B. W. Kunkle, A. B. Kuzma, C. Lage, E. J. Laukka, L. Launer, A. Lauria, C.-Y. Lee, J. Lehtisalo, O. Lerch, A. Lleó, W. Longstreth, O. Lopez, A. L. de Munain, S. Love, M. Löwemark, L. Luckcuck, K. L. Lunetta, Y. Ma, J. Macías, C. A. MacLeod, W. Maier, F. Mangialasche, M. Spallazzi, M. Marquié, R. Marshall, E. R. Martin, A. M. Montes, C. M. Rodríguez, C. Masullo, R. Mayeux, S. Mead, P. Mecocci, M. Medina, A. Meggy, S. Mehrabian, S. Mendoza, M. Menéndez-González, P. Mir, S. Moebus, M. Mol, L. Molina-Porcel, L. Montrreal, L. Morelli, F. Moreno, K. Morgan, T. Mosley, M. M. Nöthen, C. Muchnik, S. Mukherjee, B. Nacmias, T. Ngandu, G. Nicolas, B. G. Nordestgaard, R. Olaso, A. Orellana, M. Orsini, G. Ortega, A. Padovani, C. Paolo, G. Papenberg, L. Parnetti, F. Pasquier, P. Pastor, G. Peloso, A. Pérez-Cordón, J. Pérez-Tur, P. Pericard, O. Peters, Y. A. L. Pijnenburg, J. A. Pineda, G. Piñol-Ripoll, C. Pisanu, T. Polak, J. Popp, D. Posthuma, J. Priller, R. Puerta, O. Quenez, I. Quintela, J. Q. Thomassen, A. Rábano, I. Rainero, F. Rajabli, I. Ramakers, L. M. Real, M. J. T. Reinders, C. Reitz, D. Reyes-Dumeyer, P. Ridge, S. Riedel-Heller, P. Riederer, N. Roberto, E. Rodriguez-Rodriguez, A. Rongve, I. R. Allende, M. Rosende-Roca, J. L. Royo, E. Rubino, D. Rujescu, M. E. Sáez, P. Sakka, I. Saltvedt, Á. Sanabria, M. B. Sánchez-Arjona, F. Sanchez-Garcia, P. S. Juan, R. Sánchez-Valle, S. B. Sando, C. Sarnowski, C. L. Satizabal, M. Scamosci, N. Scarmeas, E. Scarpini, P. Scheltens, N. Scherbaum, M. Scherer, M. Schmid, A. Schneider, J. M. Schott, G. Selbæk, D. Seripa, M. Serrano, J. Sha, A. A. Shadrin, O. Skrobot, S. Slifer, G. J. L. Snijders, H. Soininen, V. Solfrizzi, A. Solomon, Y. Song, S. Sorbi, O. Sotolongo-Grau, G. Spalletta, A. Spottke, A. Squassina, E. Stordal, J. P. Tartan, L. Tárraga, N. Tesí, A. Thalamuthu, T. Thomas, G. Tosto, L. Traykov, L. Tremolizzo, A. Tybjærg-Hansen, A. Uitterlinden, A. Ullgren, I. Ulstein, S. Valero, O. Valladares, C. V. Broeckhoven, J. Vance, B. N. Vardarajan, A. van der Lugt, J. V. Dongen, J. van Rooij, J. van Swieten, R. Vandenberghe, F. Verhey, J.-S. Vidal, J. Vogelgsang, M. Vyhnalek, M. Wagner, D. Wallon, L.-S. Wang, R. Wang, L. Weinhold, J. Wiltfang, G. Windle, B. Woods, M. Yannakoulia, H. Zare, Y. Zhao, X. Zhang, C. Zhu, M. Zulaica, EADB, GR@ACE, DEGESCO, EADI, GERAD, Demgene, FinnGen, ADGC, CHARGE, L. A. Farrer, B. M. Psaty, M. Ghanbari, T. Raj, P. Sachdev, K. Mather, F. Jessen, M. A. Ikram, A. de Mendonça, J. Hort, M. Tsolaki, M. A. Pericak-Vance, P. Amouyel, J. Williams, R. Frikke-Schmidt, J. Clarimon, J.-F. Deleuze, G. Rossi, S. Seshadri, O. A. Andreassen, M. Ingelsson, M. Hiltunen, K. Sleegers, G. D. Schellenberg, C. M. van Duijn, R. Sims, W. M. van der Flier, A. Ruiz, A. Ramirez, J.-C. Lambert, New insights into the genetic etiology of Alzheimer's disease and related dementias. *Nat. Genet.* **54**, 412–436 (2022).
63. W. Huang, J. Zeng, L. Jia, D. Zhu, J. O'Brien, C. Ritchie, N. Shu, L. Su, Genetic risks of Alzheimer's by APOE and MAPT on cortical morphology in young healthy adults. *Brain Commun.* **5**, fcad234 (2023).
64. J. H. Lee, J. Ryan, C. Andreescu, H. Aizenstein, H. K. Lim, Brainstem morphological changes in Alzheimer's disease. *Neuroreport* **26**, 411–415 (2015).
65. P. Theofilas, A. J. Ehrenberg, S. Dunlop, A. T. Alho, A. Nguy, R. E. P. Leite, R. D. Rodriguez, M. B. Mejia, C. K. Suemoto, R. E. de Lucena Ferretti-Rebustini, L. Polichiso, C. F. Nascimento, W. W. Seeley, R. Nitrini, C. A. Pasqualucci, W. J. Filho, U. Rueb, J. Neuhaus, H. Heinsen, L. T. Grinberg, Locus coeruleus volume and cell population changes during Alzheimer's disease progression: A stereological study in human postmortem brains with potential implication for early-stage biomarker discovery. *Alzheimers Dement.* **13**, 236–246 (2017).
66. A. J. Ehrenberg, C. K. Suemoto, E. de Paula França Resende, C. Petersen, R. E. P. Leite, R. D. Rodriguez, R. E. de Lucena Ferretti-Rebustini, M. You, J. Oh, R. Nitrini, C. A. Pasqualucci, W. Jacob-Filho, J. H. Kramer, J. R. Gatchel, L. T. Grinberg, Neuropathologic correlates of psychiatric symptoms in Alzheimer's disease. *J. Alzheimers Dis.* **66**, 115–126 (2018).
67. D. A. Koolen, R. Pfundt, K. Linda, G. Beunders, H. E. Veenstra-Knol, J. H. Conta, A. M. Fortuna, G. Gillessen-Kaesbach, S. Dugan, S. Halbach, O. A. Abdul-Rahman, H. M. Winesett, W. K. Chung, M. Dalton, P. S. Dimova, T. Mattina, K. Prescott, H. Z. Zhang, H. M. Saal, J. Y. Hehir-Kwa, M. H. Willemsen, C. W. Ockeloen, M. C. Jongmans, N. Van der Aa, P. Failla, C. Barone, E. Avola, A. S. Brooks, S. G. Kant, E. H. Gerkes, H. V. Firth, K. Õunap, L. M. Bird, D. Masser-Frye, J. R. Friedman, M. A. Sokunbi, A. Dixit, M. Splitt, M. K. Kukolich, J. McGaughran, B. P. Coe, J. Flórez, N. Nadif Kasri, H. G. Brunner, E. M. Thompson, J. Gecz, C. Romano, E. E. Eichler, B. B. de Vries, The Koolen-de Vries syndrome: A phenotypic comparison of patients with a 17q21.31 microdeletion versus a KANSL1 sequence variant. *Eur. J. Hum. Genet.* **24**, 652–659 (2016).
68. J. Xu, N. Liu, E. Polemiti, L. Garcia-Mondragon, J. Tang, X. Liu, T. Lett, L. Yu, M. M. Nöthen, J. Feng, C. Yu, A. Marquand, G. Schumann, the environMENTAL Consortium, Effects of urban living environments on mental health in adults. *Nat. Med.* **29**, 1456–1467 (2023).
69. A. C. H. Chen, N. Manz, Y. Tang, M. Rangaswamy, L. Almasy, S. Kuperman, J. Nurnberger Jr., S. J. O'Connor, H. J. Edenberg, M. A. Schuckit, J. Tischfield, T. Foroud, L. J. Bierut, J. Rohrbaugh, J. P. Rice, A. Goate, V. Hesselbrock, B. Porjesz, Single-nucleotide polymorphisms in corticotropin releasing hormone receptor 1 gene (CRHR1) are associated with quantitative trait of event-related potential and alcohol dependence. *Alcohol. Clin. Exp. Res.* **34**, 988–996 (2010).
70. D. Blomeyer, J. Treutlein, G. Esser, M. H. Schmidt, G. Schumann, M. Laucht, Interaction between CRHR1 gene and stressful life events predicts adolescent heavy alcohol use. *Biol. Psychiatry* **63**, 146–151 (2008).
71. R. Daviet, G. Aydogan, K. Jagannathan, N. Spilka, P. D. Koellinger, H. R. Kranzler, G. Nave, R. R. Wetherill, Associations between alcohol consumption and gray and white matter volumes in the UK Biobank. *Nat. Commun.* **13**, 1175 (2022).
72. A. Thompson, J. Cook, H. Choquet, E. Jorgenson, J. Yin, T. Kinnunen, J. Barclay, A. P. Morris, M. Pirmohamed, Functional validity, role, and implications of heavy alcohol consumption genetic loci. *Sci. Adv.* **6**, eaay5034 (2020).
73. T. Chambers, V. Escott-Price, S. Legge, E. Baker, K. D. Singh, J. T. R. Walters, X. Caseras, R. J. L. Anney, Genetic common variants associated with cerebellar volume and their overlap with mental disorders: a study on 33,265 individuals from the UK-Biobank. *Mol. Psychiatry* **27**, 2282–2290 (2022).
74. N. C. Andreasen, R. Pierson, The role of the cerebellum in schizophrenia. *Biol. Psychiatry* **64**, 81–88 (2008).
75. T. G. M. van Erp, D. P. Hibar, J. M. Rasmussen, D. C. Glahn, G. D. Pearlson, O. A. Andreassen, I. Agartz, L. T. Westlye, U. K. Haukvik, A. M. Dale, I. Melle, C. B. Hartberg, O. Gruber, B. Kraemer, D. Zilles, G. Donohoe, S. Kelly, C. McDonald, D. W. Morris, D. M. Cannon, A. Corvin, M. W. J. Machielsen, L. Koenders, L. de Haan, D. J. Veltman, T. D. Satterthwaite, D. H. Wolf, R. C. Gur, R. E. Gur, S. G. Potkin, D. H. Mathalon, B. A. Mueller, A. Preda, F. Macciardi, S. Ehrlich, E. Walton, J. Hass, V. D. Calhoun, H. J. Bockholt, S. R. Sponheim, J. M. Shoemaker, N. E. M. van Haren, H. E. H. Pol, R. A. Ophoff, R. S. Kahn, R. Roiz-Santiañez, B. Crespo-Facorro, L. Wang, K. I. Alpert, E. G. Jönsson, R. Dimitrova, C. Bois, H. C. Whalley, A. M. McIntosh, S. M. Lawrie, R. Hashimoto, P. M. Thompson, J. A. Turner, Subcortical brain volume abnormalities in 2028 individuals with schizophrenia and 2540 healthy controls via the ENIGMA consortium. *Mol. Psychiatry* **21**, 547–553 (2016).
76. N. Okada, M. Fukunaga, K. Miura, K. Nemoto, J. Matsumoto, N. Hashimoto, M. Kiyota, K. Morita, D. Koshiyama, K. Ohi, T. Takahashi, M. Koeda, H. Yamamori, M. Fujimoto, Y. Yasuda, N. Hasegawa, H. Narita, S. Yokoyama, R. Mishima, T. Kawashima, Y. Kobayashi, D. Sasabayashi, K. Harada, M. Yamamoto, Y. Hirano, T. Itahashi, M. Nakataki, R. Hashimoto, K. K. Tha, S. Koike, T. Matsubara, G. Okada, T. G. M. van Erp, N. Jahanshad, R. Yoshimura, O. Abe, T. Onitsuka, Y. Watanabe, K. Matsuo, H. Yamasue, Y. Okamoto, M. Suzuki, J. A. Turner, P. M. Thompson, N. Ozaki, K. Kasai, R. Hashimoto, Subcortical volumetric alterations in four major psychiatric disorders: a mega-analysis study of 5604 subjects

and a volumetric data-driven approach for classification. *Mol. Psychiatry* **28**, 5206–5216 (2023).
77. Y. Jiang, C. Luo, J. Wang, L. Palaniyappan, X. Chang, S. Xiang, J. Zhang, M. Duan, H. Huang, C. Gaser, K. Nemoto, K. Miura, R. Hashimoto, L. T. Westlye, G. Richard, S. Fernandez-Cabello, N. Parker, O. A. Andreassen, T. Kircher, I. Nenadić, F. Stein, F. Thomas-Odenthal, L. Teutenberg, P. Usemann, U. Dannlowski, T. Hahn, D. Grotegerd, S. Meinert, R. Lencer, Y. Tang, T. Zhang, C. Li, W. Yue, Y. Zhang, X. Yu, E. Zhou, C.-P. Lin, S.-J. Tsai, A. L. Rodrigue, D. Glahn, G. Pearlson, J. Blangero, A. Karuk, E. Pomarol-Clotet, R. Salvador, P. Fuentes-Claramonte, M. Á. Garcia-León, G. Spalletta, F. Piras, D. Vecchio, N. Banaj, J. Cheng, Z. Liu, J. Yang, A. S. Gonul, O. Uslu, B. B. Burhanoglu, A. Uyar Demir, K. Rootes-Murdy, V. D. Calhoun, K. Sim, M. Green, Y. Quidé, Y. C. Chung, W.-S. Kim, S. R. Sponheim, C. Demro, I. S. Ramsay, F. Iasevoli, A. de Bartolomeis, A. Barone, M. Ciccarelli, A. Brunetti, S. Cocozza, G. Pontillo, M. Tranfa, M. T. M. Park, M. Kirschner, F. Georgiadis, S. Kaiser, T. E. Van Rheenen, S. L. Rossell, M. Hughes, W. Woods, S. P. Carruthers, P. Sumner, E. Ringin, F. Spaniel, A. Skoch, D. Tomecek, P. Homan, S. Homan, W. Omlor, G. Cecere, D. D. Nguyen, A. Preda, S. I. Thomopoulos, N. Jahanshad, L.-B. Cui, D. Yao, P. M. Thompson, J. A. Turner, T. G. M. van Erp, W. Cheng, J. Feng, ZIB Consortium, Neurostructural subgroup in 4291 individuals with schizophrenia identified using the subtype and stage inference algorithm. *Nat. Commun.* **15**, 5996 (2024).
78. J. R. Glausier, D. A. Lewis, Dendritic spine pathology in schizophrenia. *Neuroscience* **251**, 90–107 (2013).
79. S. Li, C. Ma, Y. Li, R. Chen, Y. Liu, L. P. Wan, Q. Xiong, C. Wang, Y. Huo, X. Dang, Y. Yang, L. Lv, X. Chen, N. Sheng, W. Li, X.-J. Luo, The schizophrenia-associated missense variant rs13107325 regulates dendritic spine density. *Transl. Psychiatry* **12**, 1–12 (2022).
80. E.-M. Stauffer, R. A. I. Bethlehem, L. Dorfschmidt, H. Won, V. Warrier, E. T. Bullmore, The genetic relationships between brain structure and schizophrenia. *Nat. Commun.* **14**, 7820 (2023).
81. Cross-Disorder Group of the Psychiatric Genomics Consortium, Genetic relationship between five psychiatric disorders estimated from genome-wide SNPs. *Nat. Genet.* **45**, 984–994 (2013).
82. M. Madre, E. J. Canales-Rodríguez, P. Fuentes-Claramonte, S. Alonso-Lana, P. Salgado-Pineda, A. Guerrero-Pedraza, N. Moro, C. Bosque, J. J. Gomar, J. Ortíz-Gil, J. M. Goikolea, C. M. Bonnin, E. Vieta, S. Sarró, T. Maristany, P. J. McKenna, R. Salvador, E. Pomarol-Clotet, Structural abnormality in schizophrenia versus bipolar disorder: A whole brain cortical thickness, surface area, volume and gyrification analyses. *Neuroimage Clin.* **25**, 102131 (2020).
83. M. Canavan, M. J. O'Donnell, Hypertension and cognitive impairment: A review of mechanisms and key concepts. *Front. Neurol.* **13**, 821135 (2022).
84. L. M. Jenkins, C. R. Garner, S. Kurian, J. P. Higgins, T. B. Parrish, S. Sedaghat, A. J. Nemeth, D. M. Lloyd-Jones, L. J. Launer, J. M. Hausdorff, L. Wang, F. A. Sorond, Cumulative blood pressure exposure, basal ganglia, and thalamic morphology in midlife. *Hypertension* **75**, 1289–1295 (2020).
85. Y. Halchenko, K. Meyer, B. Poldrack, D. Solanky, A. Wagner, J. Gors, D. MacFarlane, D. Pustina, V. Sochat, S. Ghosh, C. Mönch, C. Markiewicz, L. Waite, I. Shlyakhter, A. De La Vega, S. Hayashi, C. Häusler, J.-B. Poline, T. Kadelka, K. Skytén, D. Jarecka, D. Kennedy, T. Strauss, M. Cieslak, P. Vavra, H.-I. Ioanas, R. Schneider, M. Pflüger, J. Haxby, S. Eickhoff, M. Hanke, DataLad: Distributed system for joint management of code, data, and their relationship. *J. Open Source Softw.* **6**, 3262 (2021).
86. C. Bycroft, C. Freeman, D. Petkova, G. Band, L. T. Elliott, K. Sharp, A. Motyer, D. Vukcevic, O. Delaneau, J. O'Connell, A. Cortes, S. Welsh, A. Young, M. Effingham, G. McVean, S. Leslie, N. Allen, P. Donnelly, J. Marchini, The UK Biobank resource with deep phenotyping and genomic data. *Nature* **562**, 203–209 (2018).
87. M. Mills, N. Barban, F. C. Tropf, *An Introduction to Statistical Genetic Data Analysis* (The MIT Press, 2020).
88. J. Graffelman, V. Moreno, The mid p-value in exact tests for Hardy-Weinberg equilibrium. *Stat. Appl. Genet. Mol. Biol.* **12**, 433–448 (2013).
89. A. M. Dale, M. I. Sereno, Improved Localizadon of Cortical Activity by Combining EEG and MEG with MRI Cortical Surface Reconstruction: A Linear Approach. *J. Cogn. Neurosci.* **5**, 162–176 (1993).
90. A. M. Dale, B. Fischl, M. I. Sereno, Cortical Surface-Based Analysis: I Segmentation and Surface Reconstruction. *NeuroImage* **9**, 179–194 (1999).
91. B. Fischl, M. I. Sereno, A. M. Dale, Cortical Surface-Based Analysis: II: Inflation, Flattening, and a Surface-Based Coordinate System. *Neuroimage* **9**, 195–207 (1999).
92. B. Fischl, M. I. Sereno, R. B. H. Tootell, A. M. Dale, High-resolution intersubject averaging and a coordinate system for the cortical surface. *Hum. Brain Mapp.* **8**, 272–284 (1999).
93. B. Fischl, D. H. Salat, E. Busa, M. Albert, M. Dieterich, C. Haselgrove, A. van der Kouwe, R. Killiany, D. Kennedy, S. Klaveness, A. Montillo, N. Makris, B. Rosen, A. M. Dale, Whole Brain Segmentation: Automated Labeling of Neuroanatomical Structures in the Human Brain. *Neuron* **33**, 341–355 (2002).
94. The 1000 Genomes Project Consortium, A global reference for human genetic variation. *Nature* **526**, 68–74 (2015).
95. S. A. Lambert, L. Gil, S. Jupp, S. C. Ritchie, Y. Xu, A. Buniello, A. McMahon, G. Abraham, M. Chapman, H. Parkinson, J. Danesh, J. A. L. MacArthur, M. Inouye, The Polygenic Score Catalog as an open database for reproducibility and systematic evaluation. *Nat. Genet.* **53**, 420–425 (2021).
96. D. Lai, E. C. Johnson, S. Colbert, G. Pandey, G. Chan, L. Bauer, M. W. Francis, V. Hesselbrock, C. Kamarajan, J. Kramer, W. Kuang, S. Kuo, S. Kuperman, Y. Liu, V. McCutcheon, Z. Pang, M. H. Plawecki, M. Schuckit, J. Tischfield, L. Wetherill, Y. Zang, H. J. Edenberg, B. Porjesz, A. Agrawal, T. Foroud, Evaluating risk for alcohol use disorder: Polygenic risk scores and family history. *Alcohol. Clin. Exp. Res.* **46**, 374–383 (2022).
97. G. Molenberghs, G. Verbeke, Likelihood ratio, score, and Wald tests in a constrained parameter space. *Am. Stat.* **61**, 22–27 (2007).
98. M. S. Mufford, D. van der Meer, T. Kaufmann, O. Frei, R. Ramesar, P. M. Thompson, N. Jahanshad, R. A. Morey, O. A. Andreassen, D. J. Stein, S. Dalvie, The genetic architecture of amygdala nuclei. *Biol. Psychiatry* **95**, 72–84 (2024).

Acknowledgments: This research has been conducted using the UK Biobank Resource under application number 41655. Images of brain meshes were reproduced by permission of UKB. We further acknowledge the computing time granted by the JARA Vergabegremium and provided on the JARA Partition part of the supercomputer JURECA and the joint lab Supercomputing and Modeling for the Human Brain at Forschungszentrum Jülich. **Funding:** This work was supported by the following: Helmholtz Imaging grant (NimRLS, ZT-I-PF-4-010) (to S.B.E., J.W., K.O., and K.R.P.) and Helmholtz Imaging grant (BrainShapes, ZT-I-PF-4-062) (to S.B.E., J.W., K.O., and K.R.P.). **Author contributions:** Conceptualization: S.A.P., S.B.E., J.W., K.O., and K.P. Methodology: S.A.P., K.O., and K.P. Investigation: S.A.P. and K.O. Visualization: S.A.P. Supervision: S.B.E., J.W., K.O., and K.P. Writing—original draft: S.A.P., K.O., and K.P. Writing—review and editing: S.A.P., F.H., F.R., S.B.E., K.O., and K.P. Resources: F.H., S.B.E., J.W., and K.P. Data curation: S.A.P., F.H., and K.P. Formal analysis: S.A.P., F.H., K.O., and K.P. Software: S.A.P., F.H., F.R., and K.P. Funding acquisition: S.B.E., J.W., K.O., and K.P. Project administration: S.B.E., J.W., K.O., and K.P. Validation: S.A.P., F.R., K.O., and K.P. **Competing interests:** The authors declare that they have no competing interests. **Data and materials availability:** All data needed to evaluate the conclusions in the paper are present in the paper and/or the Supplementary Materials. This research has been conducted using the UK Biobank Resource under application number 41655. These data can be provided by UKB pending scientific review and a completed material transfer agreement. Requests for the data should be submitted to the UKB: www.ukbiobank.ac.uk. Specific UKB data field codes are given in the Materials and Methods. Other publicly available data sources and applications are cited in the Materials and Methods. Our MOSTest summary statistics are made available online via the GWAS catalog (www.ebi.ac.uk/gwas/) under the consecutive accession numbers from GCST90559206 to GCST90559227. FUMA results and scripts can be found on Zenodo (https://doi.org/10.5281/zenodo.14987679). This study used openly available software and codes, specifically Plink (www.cog-genomics.org/plink/), FUMA (https://fuma.ctglab.nl/), LDtrait (https://ldlink.nih.gov/?tab=ldtrait), and MAGMA (https://ctg.cncr.nl/software/magma; also implemented in FUMA), as well as BrainPrint (https://github.com/Deep-MI/BrainPrint), MOSTest (https://github.com/precimed/mostest), SCORE (https://github.com/sriramlab/SCORE), and PoPS (https://github.com/FinucaneLab/pops), for which we provide a permanent archive on Zenodo (https://doi.org/10.5281/zenodo.14987679). For plotting, we used fastman (https://github.com/kaustubhad/fastman), ggseq3d (https://CRAN.R-project.org/package=ggseg3d), circlize (https://CRAN.R-project.org/package=circlize), and yacca (https://CRAN.R-project.org/package=yacca).We further used Affinity Designer for figure design.

Submitted 20 June 2024
Accepted 9 May 2025
Published 13 June 2025
10.1126/sciadv.adr1644